

Supergene gold transformation:
Secondary and nano-particulate gold
from northern Finland

Thesis submitted in accordance with the requirements of the University of
Adelaide for an Honours Degree in Geology

Paige Sawley
November 2014



THE UNIVERSITY
of ADELAIDE

SUPERGENE GOLD TRANSFORMATION: SECONDARY AND NANO-PARTICULATE GOLD FROM NORTHERN FINLAND

SUPERGENE GOLD TRANSFORMATION

ABSTRACT

The transformation of gold (Au) in many supergene environments is driven by (bio)geochemical processes. This study assesses the link between surface morphologies of Au grains and supergene transformation processes in arctic settings. Gold grains were collected from nine sites across two localities in northern Finland, *i.e.*, Ivalojoiki and Lemmenjoki. Sites were chosen based on contrasting elevations and settings, from glacial till to alluvial. Gold grains were studied using field emission scanning electron microscopy (FEG-SEM), focused ion beam-scanning electron microscopy (FIB-SEM) coupled with Energy Dispersive X-ray Spectroscopy (EDXS), and electron microprobe analyses (EPMA). Gold grains from all sites displayed supergene transformation features, *i.e.*, morphotypes indicative of Au and Ag dissolution, as well as Au aggregation. The latter included a variety of secondary Au morphotypes, such as nano-particles and μ -crystals, sheet-like Au and branched Au networks. Dissolution features on grains from high organic matter environments suggest fulvic and humic acids are important contributors in the transformation of Au. Secondary Au occurs as part of the polymorphic layer. In addition to the secondary Au, the polymorphic layer consists of active microbial biofilms, organic matter and biominerals suggestive of remnant biofilms, as well as aluminosilicates, iron-sulfides and oxides. Bacterial cells and putative fungal hyphae were closely associated with Au nano-particles, suggesting that Au biomineralisation is an important factor in the transformation of Au. In conclusion, surface morphologies of Au grains from Finland are the result of supergene (bio)geochemical transformations occurring in the arctic environment.

KEYWORDS

Gold, supergene, Finland, arctic, nano-particles, biofilm

TABLE OF CONTENTS

Supergene gold transformation: Secondary and nano-particulate gold from northern Finland	i
Supergene gold transformation	i
Abstract	i
Keywords	i
1. List of Figures	2
2. List of Tables	3
3. Introduction	4
4. Geological Setting	6
5. Methods	8
6. Observations and Results	10
5.1 Gold grains from Ivalojoiki, Finland	10
5.1.1 Ivalojoiki 1	10
5.1.2 Aila's claim	13
5.1.3 Risto's Claim	15
5.2 Gold grains for Lemmenjoki, Finland	17
5.2.1 Jäkäläpää claim	17
5.2.2 (Miessi) Turkka's Claim	20
5.2.3 (Miessi) Pekka's Claim	22
5.2.4 (Miessi) Raimo's Claim	24
5.2.5 Kaarreoja Claim	25
5.2.6 (Miessi) Ami's Claim	27
7. Discussion	29
8. Conclusions	34
9. Acknowledgments	35
10. References	35
Appendix A: Methods	39
Appendix B: Supplementary Figures	45

1. LIST OF FIGURES

Figure 1: Finland sample site locations; insert Lemmenjoki, (1) (Miessi) Turkka's Claim, (2) Jäkäläpää Claim, (3) (Miessi) Pekka's Claim, (4) (Miessi) Raimo's Claim, (5) Kaarreoja Claim, (6) (Miessi) Ami's Claim. Insert Ivalojoiki. (1) Ivalojoiki 1, (2) Aila's Claim, (3) Risto's Claim. Modified after Google Earth.	7
Figure 2: Backscatter electron (BSE, a, b) and scanning electron (SE, c, d) micrographs and EDXS maps (e–h) of Au grains from Ivalojoiki 1, Ivalojoiki, Finland. (a) Micrograph showing a typical irregular Au grain with rounded and partially folded edges; (b) conglomerate of Au μ -crystals surrounded by Au nano-particles in the polymorphic layer; (c) micrograph showing the polymorphic layer described in (b); (d) a sheet-like, secondary Au plate; (e–h) EDXS maps of Au, Ag, Fe and Si concentrations (wt. %)...	11
Figure 3: Electron microprobe maps of Au, Ag and Fe concentrations in a polished section of two Au grains from Ivalojoiki 1, Ivalojoiki, Finland. (a) Maximum concentrations of Au 100 wt.%; (b) maximum concentration of Ag 13.37 wt.%; (c) maximum concentrations of Fe 35.50 wt.%.	12
Figure 4: Electron micrographs of Au grains from Ivalojoiki 1, Ivalojoiki, Finland, showing (a) typical features of the polymorphic layer, with bacterial cell (arrow); (b) conglomerate of Au μ -crystals, surrounded by Au nano-particles and bacterial cell (arrow) dispersed through the polymorphic layer; (c) a bacterial, rod-shaped cell attached by pili; (d) a bacterial rod-shaped cell surrounded by Au nano-particles (arrows).	13
Figure 5: BSE (a, c–e) and SE (b) micrographs of Au grains from Aila's Claim, Ivalojoiki, Finland, showing (a) a typical Au grain with rounded and partially folded edges; (b) the physically damaged grain surfaces; (c) dissolution pits on the grain surface and budding Au forming bridging structures; (d) Au μ -crystals and nano-particles dispersed through the polymorphic layer; (e) triangular-shaped, flat Au crystal.	14
Figure 6: SE (a) and BSE (b–d) micrographs of Au grains from Risto's Claim, Ivalojoiki, Finland, showing (a) a typical flattened grain with rounded edges; (b) the physically damaged grain surfaces; (c) Au dissolving into the polymorphic layer, (d) the highly transformed grain surfaces with few Au nano-particles and budding structures.	16
Figure 7: SE (a, d) and BSE (b, c) micrographs of Au grains from Jäkäläpää Claim, Lemmenjoki, Finland, showing (a) a branching Au grain with sub-rounded edges; (b) budding Au and extensive Au nano-particles dispersed through the polymorphic layer; (c) Au μ -crystals and Au nano-particles accumulating in a Ti rich part of the matrix; (d) a pyrite particle (red arrow) and a biomineral (orange arrow).	17
Figure 8: Electron micrographs (a, b) and EDSX maps (c–h) of an Au grain from Jäkäläpää Claim, Lemmenjoki, Finland, showing (a) typical surface features of the grains; (b) FIB-SEM micrograph showing a milled section through a layer of material similar to that shown in (a); (c–d) EDXS maps of Au, Ag, Fe, C, O and Ti concentrations (wt.%) of the milled sections shown in (b).	18
Figure 9: Electron microprobe maps of Au, Ag and Fe concentrations in a polished section of two Au grains from Jäkäläpää Claim, Lemmenjoki, Finland. (a) Maximum	

concentrations of Au 100 wt.%; (b) maximum concentration of Ag 46.07 wt.%; (c) maximum concentrations of Fe 32.07 wt.%.	20
Figure 10: BSE (a, b, d) and SE (c) micrographs and an electron microprobe map of Au grains from (Miessi) Turkka's Claim, Lemmenjoki, Finland showing (a) a wire Au grain with rounded edges; (b) the typical textured grain surface; (c) a network of biological nano-wires (arrows) running through the polymorphic layer; (d) triangular and spherical shaped Au nano-particles; (e) minimum concentrations of Au 60 wt.%, maximum concentrations of Au 100 wt.%.	21
Figure 11: BSE (a, d) and SE (b, c) micrographs of Au grains from (Miessi) Pekka's Claim, Lemmenjoki, Finland, showing (a) an elongate grain with sub-rounded edges; (b) the typical features of the polymorphic layer; (c) bacterial, rod-shaped cells (arrows) on the grain surface; (d) Au nano-particles dispersed through the polymorphic layer. . .	23
Figure 12: SE (a–c) and BSE (d, e) micrographs of Au grains from (Miessi) Raimo's Claim, Lemmenjoki, Finland, showing (a) a flattened, branched grain; (b) biological material on the physically damaged surfaces; (c) a cluster of rod-shaped bacterial cells on the surface of the polymorphic layer; (d) the bacterial cells shown in (c) surrounded by Au nano-particles; (e) budding Au forming bridging structures.	25
Figure 13: BSE micrographs (a, b) and electron microprobe maps (c–h) of Au grains from Kaarreoja Claim, Lemmenjoki, Finland showing (a) a wire Au grain with rounded edges; (b) Au nano-particles dispersed through the polymorphic layer; electron microprobe maps of Au (c, e, g; maximum concentration 100 wt.%) and Ag (d, f, h; maximum concentration 23.88 wt.%). Note the lack of Ag at enriched Au rims.	26
Figure 14: BSE (a–c) micrographs and electron microprobe maps (d, e) of Au grains from (Miessi) Ami's Claim, Lemmenjoki, Finland showing (a) an irregular Au grain with sub-rounded edges; (b) typical surface features of the grains; (c) increased magnification of Au nano-particles, area highlighted in (b); (d, e) electron microprobe maps of Au (d; maximum concentrations 100 wt.%) and Ag (e; maximum concentrations 11.66 wt.%).	28

2. LIST OF TABLES

Table 1: Summary of the environmental properties at the sampling sites.	8
--	---

3. INTRODUCTION

Gold (Au) is rare (~1 ppb) in the Earth's crust (Hough *et al.* 2009). One of the most important sources of Au is alluvial placer deposits (Youngson & Craw 1993). Alluvial Au is most commonly found micrometer to millimetres in size (Hough *et al.* 2009).

Under surface conditions and in aqueous solutions, Au can occur in three forms; colloidal [Au (0)], aurous [Au (I)] or auric [Au (III)] (Southam *et al.* 2009).

Primary Au is Au that has originated from high temperature systems (Fairbrother *et al.* 2012). It is most commonly an Au/Ag alloy, containing between 5–20% Ag (Hough *et al.* 2009). Physical erosion of host material results in primary Au being deposited in supergene placers (Fairbrother *et al.* 2012). Secondary Au occurs on the surface of primary Au and usually has a high purity (>99 wt. % Au). Many Au grains recovered in placer environments display a core of Au-Ag and have a partial or complete rim of high purity Au (*e.g.* Groen *et al.* 1990, McCready *et al.* 2003, Fairbrother *et al.* 2012, Reith *et al.* 2012). Secondary Au can have a range of morphologies including wire Au, Au nanoparticles and μ -crystals, bacteriomorphic Au and sheet-like Au (Falconer *et al.* 2006, Reith *et al.* 2006, Hough *et al.* 2011). Nano-particulate Au also have a variety of morphologies including triangle, spherical, hexagonal and octahedral (Fairbrother *et al.* 2013).

There has been debate on whether the development of Au grains in supergene environments is driven by detrital (Minter *et al.* 1993, Hough *et al.* 2007) or chemical accretionary (Youngson & Craw 1993) processes. A recent model by Fairbrother *et al.* (2012) has integrated both to create a model of supergene processes for the transformation of Au grains. In this model, the physically eroded primary Au, now in the supergene environment, experiences Ag de-alloying and Au dissolution. De-alloying

is the selective leaching of less noble elements (*e.g.* Ag) and results in nano-porous Au structures (Schofield *et al.* 2008). Gold becomes soluble in surface waters by forming complexes with thiosulphate, chloride, halides, organic ligands and cyanide (Reith *et al.* 2007). Abiogenic and biogenic processes then re-precipitate the complexed Au, forming secondary Au.

Evaporation is an abiogenic process that is thought to promote Au precipitation. This is because Au nano-plates have been shown to be intergrown with evaporite minerals, (Hough *et al.* 2008). However, biogenically mediated precipitation has also well documented, with bacteria shown to accumulate and precipitate Au (*e.g.*, Karthikeyan & Beveridge 2002, Reith & McPhail 2006, Fairbrother *et al.* 2013). Gold (III) complexes however, can be highly toxic to microbes (Nam *et al.* 2014). For example, cyanobacteria have shown to precipitate Au nano-particles and form Au platelets (Lengke *et al.* 2006). The Au enters the cell in its Au (III) form and then is reduced to Au (0). However, before being reduced, the toxic Au (III) is thought to degraded the cells, resulting in further Au precipitation (Lengke *et al.* 2006). Some bacteria have developed mechanisms against the Au (III) toxic effects (*e.g.* Reith & McPhail 2006, Checa *et al.* 2007, Reith *et al.* 2013), and in same case have used Au to its advantage. This includes using Au-complexing ligands to gain metabolic energy and using Au as a metal centre in enzymes (Southam *et al.* 2009).

Most Au grains are partially covered by a polymorphic layer. This layer is composed of microbial biofilms, Au nano-particles and bacteriomorphic Au, clay-, iron- and silicate minerals (Reith *et al.* 2010). The relationship between Au nano-particles and biofilms suggests that biofilms may influence the rate of Au mobilisation and re-precipitation.

Few time constraints on secondary processes are yet to be established. Gold grains from Precambrian environments in arid Australia and Palaeozoic to Oligocene temperate environments in New Zealand have shown to display extensive secondary features (Falconer *et al.* 2006, Fairbrother *et al.* 2012, Reith *et al.* 2012). Grains from these environments have also shown that Au transformation is biologically mediated (Reith *et al.* 2010, Fairbrother *et al.* 2012, Reith *et al.* 2012). Whether or not these processes occur in younger, arctic environments is unknown. Hence, the aim of this study is to assess the link between surface morphologies of gold grains and supergene transformation processes in arctic settings. Areas of specific interest are: (i) if microbial biofilms and polymorphic layers exist on the grains; (ii) if there are Au nano-particles within these layers; and (iii) the morphologies and chemical composition of the grains. To achieve this, gold grains from two localities in northern Finland were studied using advanced micro-analytical techniques, including field emission scanning electron microscopy (FEG-SEM), focused ion beam-scanning electron microscopy (FIB-SEM) coupled with Energy Dispersive X-ray Spectroscopy (EDXS), and electron microprobe analyses (EPMA).

4. GEOLOGICAL SETTING

The sites studied are located in the Ivalojoiki and Lemmenjoki districts, approximately 20 km east and 80 km southwest of Inari, respectively, in northern Lapland, Finland. The maximum temperature in the summer is 18°C and the minimum temperature is -18°C in the winter. The annual rainfall is approximately 500–550 mm (Finnish Meteorological Institute 2014). Approximately 10% of northern Finland is covered by water bodies and 30% is covered by peat lands (Stigzelius 1977). Gold washing has

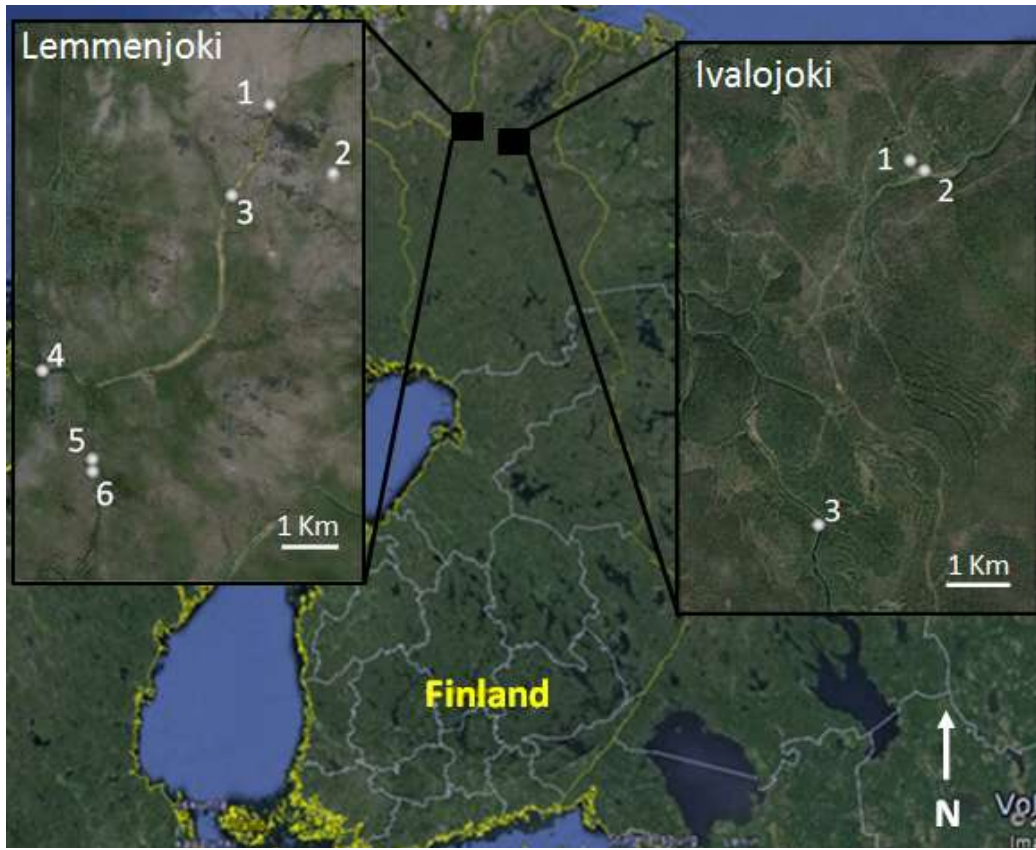


Figure 1: Finland sample site locations; insert Lemmenjoki, (1) (Miessi) Turkka's Claim, (2) Jäkäläpää Claim, (3) (Miessi) Pekka's Claim, (4) (Miessi) Raimo's Claim, (5) Kaarreoja Claim, (6) (Miessi) Ami's Claim. Insert Ivalojoiki. (1) Ivalojoiki 1, (2) Aila's Claim, (3) Risto's Claim. Modified after Google Earth.

been occurring along the Inari river since the 19th century (Puustinen 1991, Kojonen *et al.* 2005). The size of Au grains can be a very fine dust to nuggets weighing hundreds of grams (Puustinen 1991).

Geologically, Ivalojoiki and Lemmenjoki are located in the southern part of a granulite belt (Saarnisto *et al.* 1991, Kojonen *et al.* 2005). The complex was metamorphosed during the Svecokarelian Orogeny (~1.9 Ga), under granulite conditions (Saarnisto *et al.* 1991, Tuisku *et al.* 2006). Northern Finland was glaciated during the Pleistocene (Stigzelius 1977). Deglaciation began in northern Finland approximate 11,600 years ago (Lunkka *et al.* 2004). During deglaciation, river valleys acted as meltwater channels. Most of the Au fields are interpreted as glaciofluvial placers, varying in size and

composed of poorly sorted sediments (Saarnisto *et al.* 1991, Kinnunen 1996). Gold has also been discovered in river terraces, bottom sands and tills (Saarnisto *et al.* 1991). Gold samples were taken from nine main sites, all of which are currently mining claims. Three sites were within the Ivalojoiki district and six were within the Lemmenjoki district (Fig. 1). Sites were chosen based on contrasting elevations and settings (Table 1).

Table 1: Summary of the environmental properties at the sampling sites.

Sample Name	District	GPS coordinates	Approximate elevation relative to sea level (m)	Setting	Depth of sample (m)
Ivalojoiki 1	Ivalojoiki	35W, N68 27'27.6" E26 56'49.4"	260	Till	2
Aila's Claim	Ivalojoiki	35W, N68 27'31.6" E26 56'34.8"	270	Till	2-3
Risto's Claim	Ivalojoiki	35W, N68 25'12.0" E26 54'50.0"	230	Alluvial	N/A
Jäkäläpää Claim	Lemmenjoki	35W, N68 41'54.0" E25 43'42.1"	450	Till	1
(Miessi) Turkka's Claim	Lemmenjoki	35W, N68 42'31.1" E25 42'01.2"	440	Till with alluvial reworking	N/A
(Miessi) Pekka's Claim	Lemmenjoki	35W, N68 41'40.0" E25 41'08.7"	403	Till with alluvial reworking	1
(Miessi) Raimo's Claim	Lemmenjoki	35W, N68 39'54.9" E25 36'18.3"	438	Till with alluvial reworking	n.r.
Kaarreoja Claim	Lemmenjoki	35W, N68 39'06.0" E25 37'45.4"	358	Till	3
(Miessi) Ami's Claim	Lemmenjoki	35W, N68 38'59.0" E25 37'46.7"	361	n. r.	N/A

5. METHODS

Gold grains from the Ivalojoiki and Lemmenjoki districts were collected in August 2013.

Grains were collected from each site according to a field sterile procedure aimed at preventing contamination and preserving delicate structures (Reith *et al.* 2010). Gold

grains were washed and stored in 1–2 ml of sterile physiological solution (0.9 wt. % NaCl) and were kept cool whilst transported to the laboratory.

Gold grains from each site were either air dried or dehydrated. Dehydration was completed using increments of ethanol (70%, 90% and 100%) and then 100% Hexamethyldisilazane (HDMS), before drying. Ten uncoated, air dried samples and 28 dehydrated, C-coated samples were analysed using field emission scanning electron microscopes (Quanta 450, Phillips XL-30, Adelaide Microscopy, University of Adelaide). Images of surface features were collected in secondary electron and backscatter imaging mode at 5kV and 20kV, respectively. Selected samples were further analysed using a focus ion beam secondary electron microscope (FIB-SEM; Helios NanoLab DualBeam). Images of the surface features were collected at 2 to 20kV and 86pA, with sectioning and cleaning at 20kV and 9.7pA. Sectioning was completed to observe the processes occurring within the polymorphic layers. The instrument was equipped with an Energy Dispersive X-ray Spectroscopy (EDXS); this was used to collect element maps across grain surfaces and milled sections.

Other Au grains were set in epoxy resin, polished with 1 µm diamond paste and coated with a 15 nm thick carbon film. One to four grains from each site were quantitatively mapped using a Cameca SXFive Electron Microprobe running the PeakSite software for instrument control, and Probe for EPMA™ for data acquisition and processing (Adelaide Microscopy, University of Adelaide). The SXFive was equipped with five WLD X-Ray detectors. The MAN background correction and elemental pixel quantification were performed in CalcImage, and false colourisation and formatting was completed in Surfer™. Analysis was conducted at 20kV and 150nA. The grains were analysed for (detection limit range in parenthesis in wt.%): Au(0.99–2.9), Ag(0.45–

0.49), Cu(0.25–0.61), As(0.43–0.60), Zn(0.33–0.85), Ti(0.09–0.15), Fe(0.18–0.39), S(0.16–0.17). All elements were calibrated on a mixture of minerals and pure metal standards from Astimex and P&H. Cu, Fe and S were calibrated on chalcopyrite; As on gallium arsenide; Zn on sphalerite; Ag on Telluride; Ti on Rutile; and Au on a pure metal standard.

6. OBSERVATIONS AND RESULTS

5.1 Gold grains from Ivalojoiki, Finland

5.1.1 IVALOJOKI 1

Grains from Ivalojoiki 1 ranged in size from approximately 1.5 to 1.8 mm in diameter. Grains were irregular and had rounded edges that can be partially folded (Fig. 2a). Other than folded edge, there was little physical damage to the grains.

Nano-particulate Au and conglomerates of Au μ -crystals were common throughout a polymorphic layer (Fig. 2b). Sheet-like Au, resembling the shape of triangles, were also observed (Fig. 2c). An EDXS element map across a section of the grain surface and polymorphic layer showed Au dispersed through the layer (Fig. 2e). Silver did not appear with Au in the polymorphic layer (Fig. 2f). The polymorphic layer consisted of Fe, Si, (Fig. 2g, h), C, O, Na, Mg, Al, and P and occurred mostly in the topographic lows.

Three Au grains were quantitatively mapped using the Cameca SXFive Electron Microprobe. The element maps across grain interiors showed an Au enriched rim that can be as thick as 40 μ m (Fig. 3a). Areas of greatest thickness occurred partially around

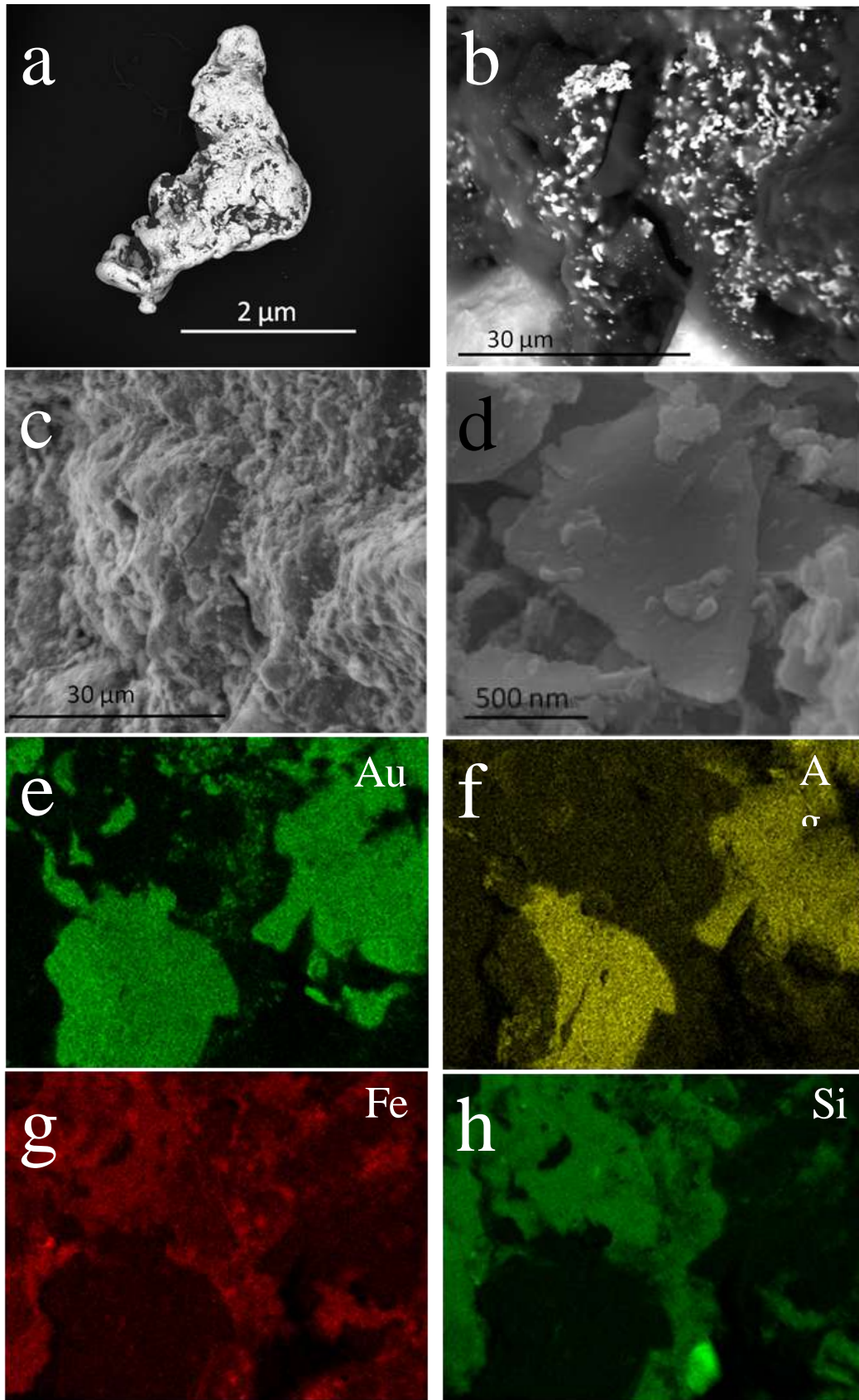


Figure 2: Backscatter electron (BSE, a, b) and scanning electron (SE, c, d) micrographs and EDXS maps (e-h) of Au grains from Ivalojoiki 1, Ivalojoiki, Finland. (a) Micrograph showing a typical irregular Au grain with rounded and partially folded edges; (b) conglomerate of Au μ -crystals surrounded by Au nano-particles in the polymorphic layer; (c) micrograph showing the polymorphic layer described in (b); (d) a sheet-like, secondary Au plate; (e-h) EDXS maps of Au, Ag, Fe and Si concentrations (wt. %).

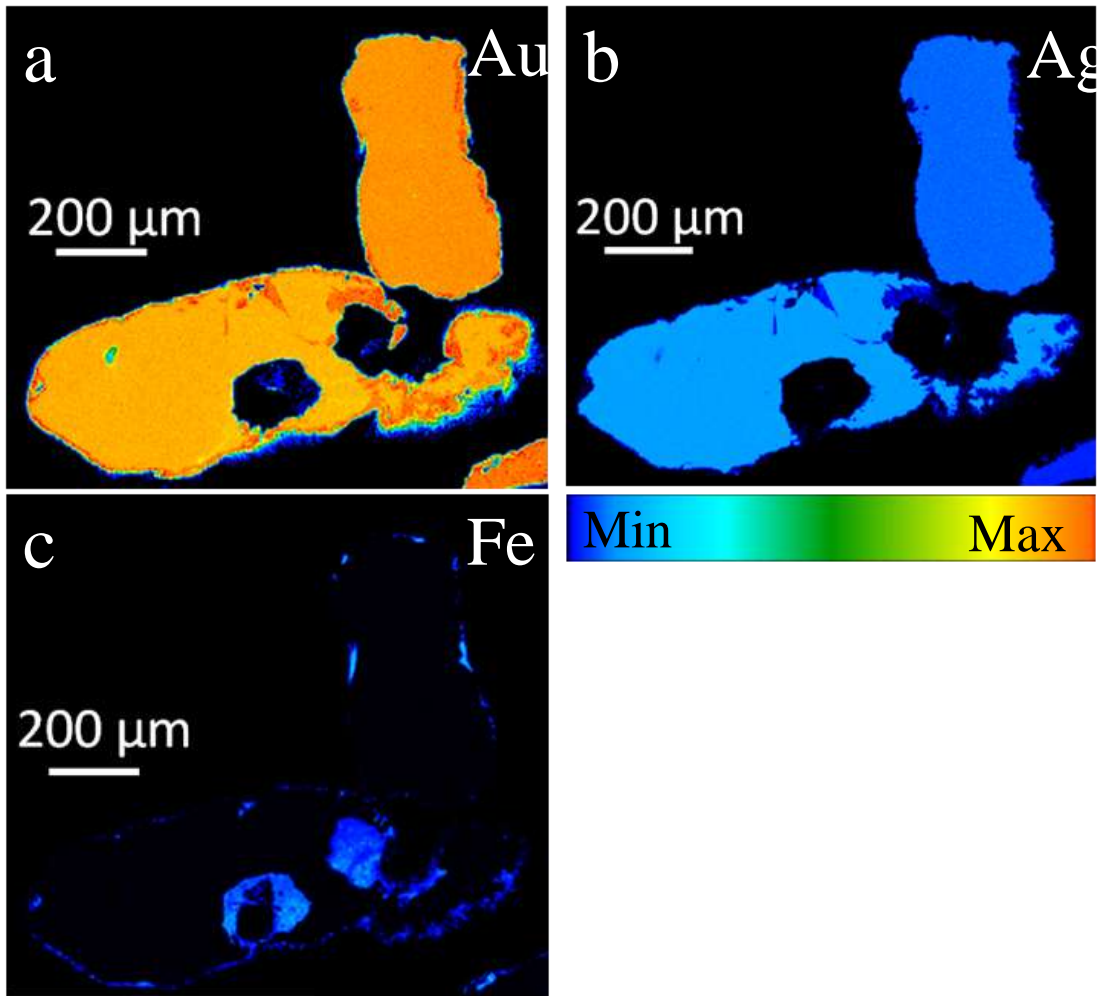


Figure 3: Electron microprobe maps of Au, Ag and Fe concentrations in a polished section of two Au grains from Ivalojoiki 1, Ivalojoiki, Finland. (a) Maximum concentrations of Au 100 wt.%; (b) maximum concentration of Ag 13.37 wt.%; (c) maximum concentrations of Fe 35.50 wt.%.

inclusions. Other grains showed partial or no enrichment of Au at the margins. Gold concentrations on the rim of the grains can be as high as 100% Au, with core concentrations varied, but always >85% Au. Silver concentrations also varied, with minimum concentrations at the Au enriched rims. The Ag concentration within the grain core can be as high as 13.38% Ag (Fig. 3b), or in one grain, below detection limit of 0.47% Ag. Trace elements were also analysed. Grain margins showed maximum Fe concentrations, as high as 35.50% Fe (Fig. 3c). Elements below detection limit included Ti, Zn, As and Cu. There were inclusions ranging from 40 to 200 μm.

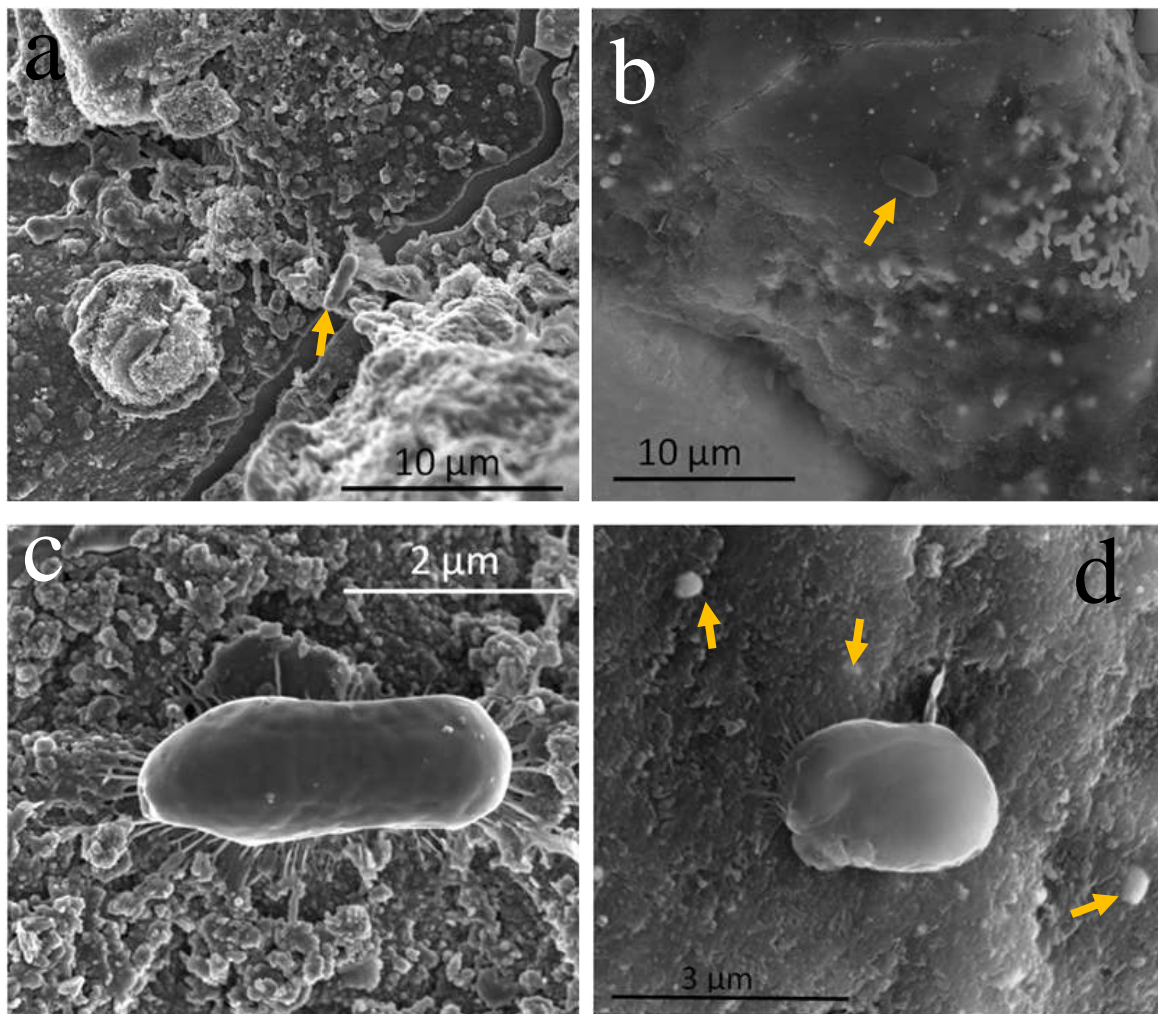


Figure 4: Electron micrographs of Au grains from Ivalojoiki 1, Ivalojoiki, Finland, showing (a) typical features of the polymorphic layer, with bacterial cell (arrow); (b) conglomerate of Au μ -crystals, surrounded by Au nano-particles and bacterial cell (arrow) dispersed through the polymorphic layer; (c) a bacterial, rod-shaped cell attached by pili; (d) a bacterial rod-shaped cell surrounded by Au nano-particles (arrows).

Bacterial cells were observed in the polymorphic layer (Fig. 4a, b) and can be surrounded by what appeared to be fungal hyphae. Singular rod-shaped bacterial cells were observed in relatively protected areas on the grains, attached by pili (Fig. 4c, d). Cells were up to 3 μ m in length and can be surrounded by nano-particles (Fig. 4d).

5.1.2 AILA'S CLAIM

Grains from Aila's Claim ranged in size from approximately 0.8 to 1.1 mm in diameter.

Grains were commonly irregular but can be branching. Grain edges had been

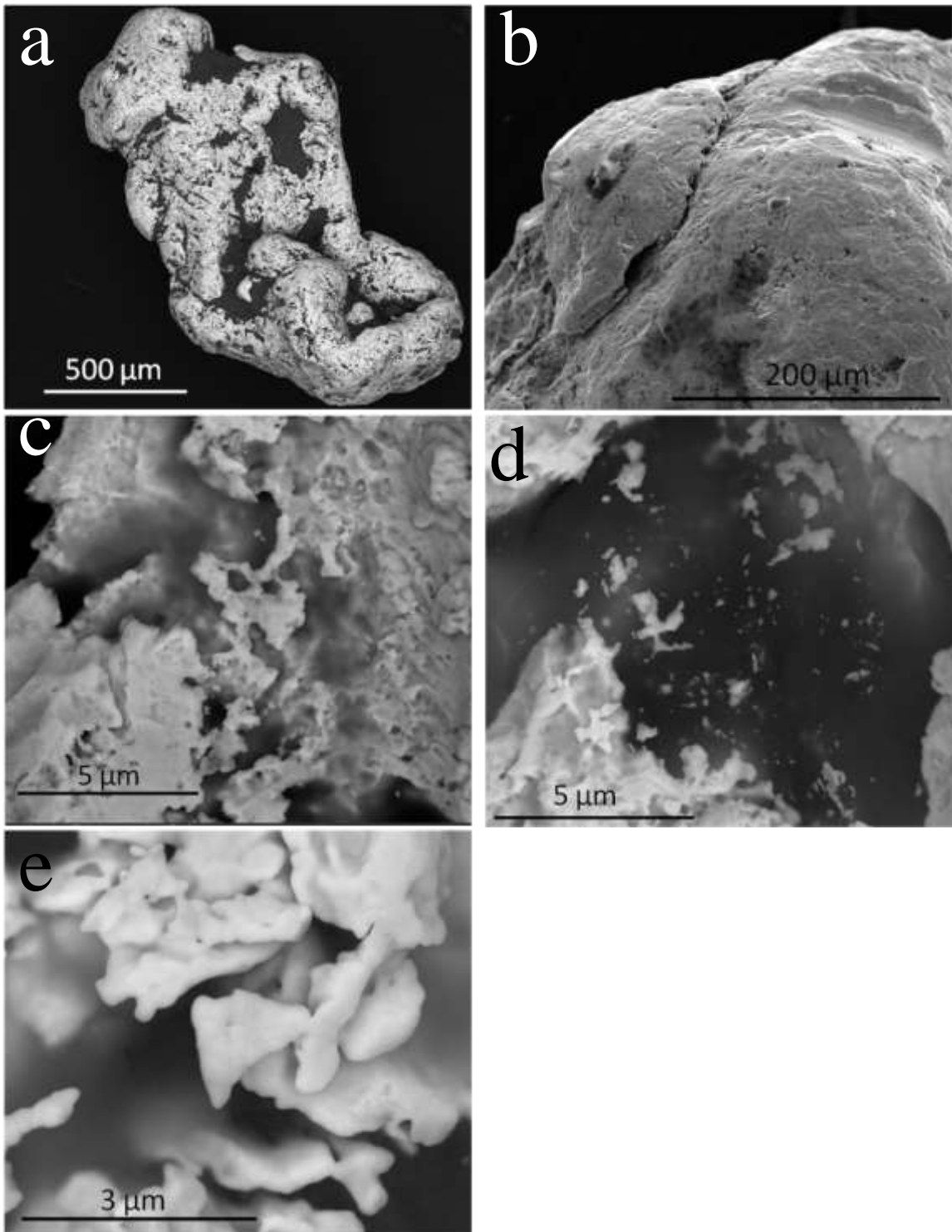


Figure 5: BSE (a, c–e) and SE (b) micrographs of Au grains from Aila’s Claim, Ivalo, Finland, showing (a) a typical Au grain with rounded and partially folded edges; (b) the physically damaged grain surfaces; (c) dissolution pits on the grain surface and budding Au forming bridging structures; (d) Au μ -crystals and nano-particles dispersed through the polymorphic layer; (e) triangular-shaped, flat Au crystal.

rounded and folded (Fig. 5a). Grains appeared to be battered and striations were

common on the surface (Fig. 5b). Pitted surfaces were observed on the grain (Fig. 5c).

Similar to Ivalojoiki 1, grains were partially covered by a polymorphic layer, predominantly in the topographic lows and cavities. Budding Au can appear to be creating bridging structures over the polymorphic layer (Fig. 5c). The polymorphic layer contained Au μ -crystals (Fig. 5d), Au nano-particles, sheet-like Au (Fig. 5e) and biological material.

Rod-shaped cells can be in a cluster or singular. They were usually protected in larger cavities and could appear along with relics of diatoms. Cell size ranged between 2.5 to 3.5 μm and can be surrounded by nano-particles.

Three element maps across grain interiors showed partially developed Au enriched rims on some grains and others that were completely homogenous. The Au concentrations at the rim of the grain can be as high as 100% Au, with varied core concentrations, always >86% Au. The Ag concentrations within the grain core can be as high as 10.09% Ag or below the detection limit of 0.47% Ag. Trace elements were also analysed, showing higher concentrations of S, Zn and Cu inconsistently along the grain margins.

Concentrations of S along the margins, and with minor amounts in the core, had a maximum value 1.69% S. Other maximum values were 1.02% Zn and 0.78% Cu.

Elements below detection limit include As. Inclusions were found internally and on the edges of grains. They can range in size from 80 to 120 μm . Inclusions on the edges can have Fe concentrations as high as 21.18% Fe. Internal inclusion showed to contain Ti with a maximum concentration of 35.23% Ti.

5.1.3 RISTO'S CLAIM

Grains from Risto's Claim were between 0.20 to 0.25 mm in diameter. Grains can be equant or irregular (Fig. 6a). They were flattened, with sub-rounded to rounded edges.

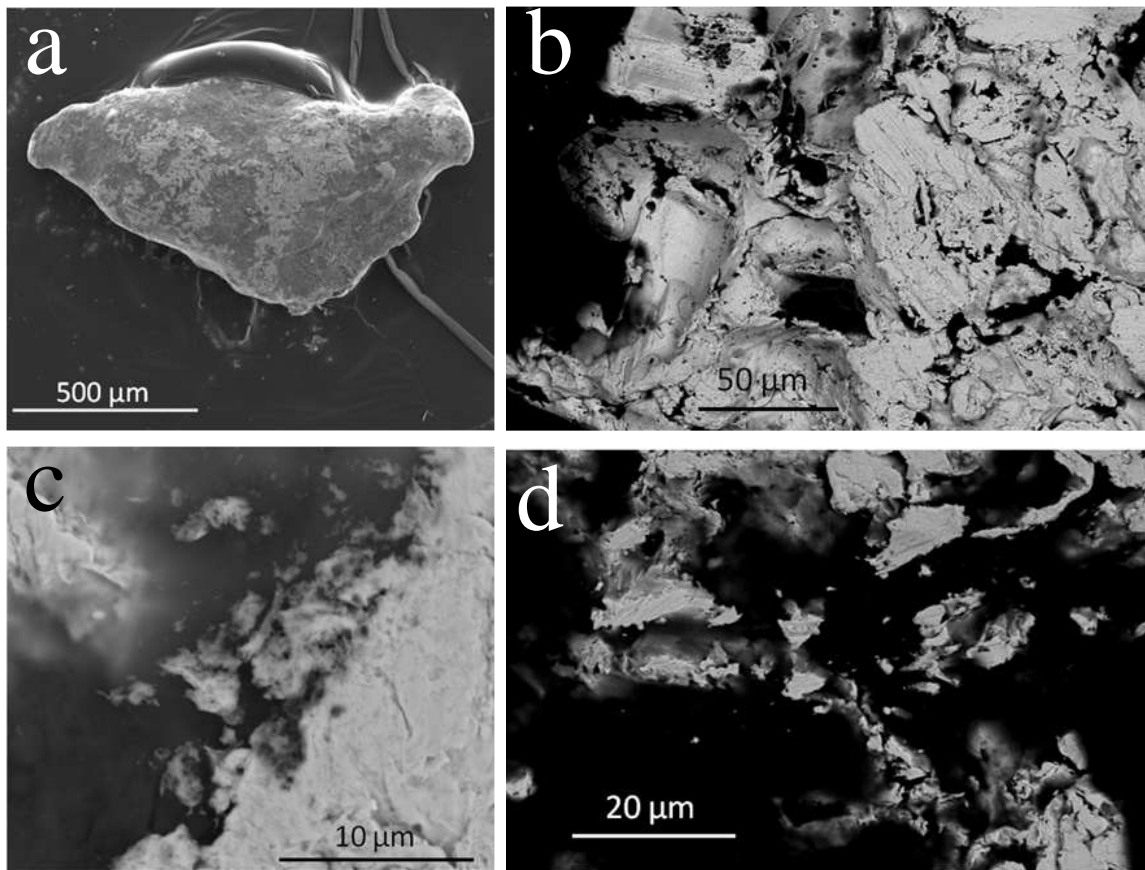


Figure 6: SE (a) and BSE (b–d) micrographs of Au grains from Risto’s Claim, Ivalojoiki, Finland, showing (a) a typical flattened grain with rounded edges; (b) the physically damaged grain surfaces; (c) Au dissolving into the polymorphic layer, (d) the highly transformed grain surfaces with few Au nano-particles and budding structures.

The gold surface was mostly smooth but can have randomly orientated carved, striated channels. Pits were seen in areas that were more physically damaged (Fig. 6b).

A polymorphic layer can cover a large proportion of the grain or just partially cover areas, again remaining in the topographic lows. Gold can appear to be dissolving into the polymorphic layer (Fig. 6c) and branching Au was observed. This site had fewer nano-particulate and μ -crystals dispersed in the layer than grains from other Ivalojoiki sites (Fig. 6d).

Extensive biological material was observed over grain surfaces, composed of C, N and O. This material was found in both the polymorphic layer and in direct contact with the Au grain surface.

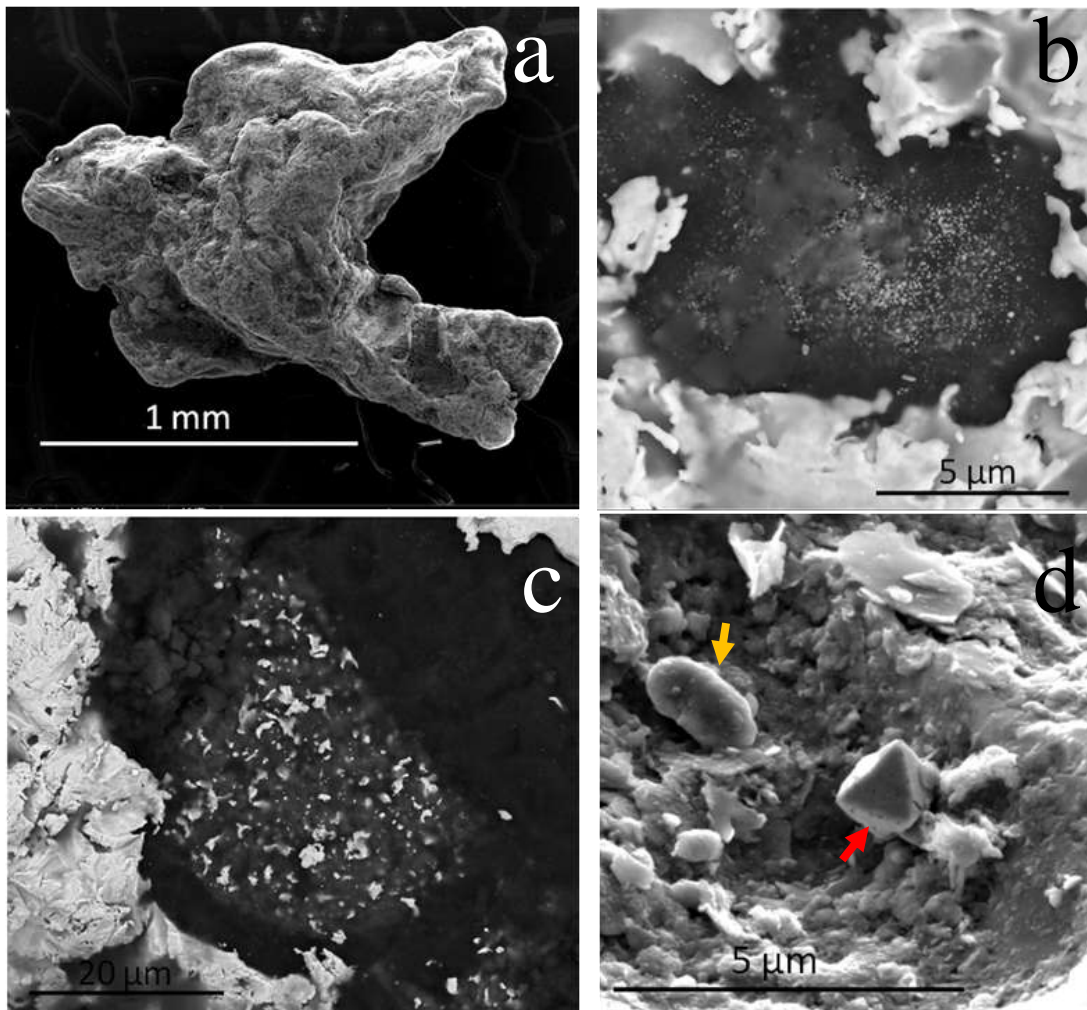


Figure 7: SE (a, d) and BSE (b, c) micrographs of Au grains from Jäkäläpää Claim, Lemmenjoki, Finland, showing (a) a branching Au grain with sub-rounded edges; (b) budding Au and extensive Au nano-particles dispersed through the polymorphic layer; (c) Au μ -crystals and Au nano-particles accumulating in a Ti rich part of the matrix; (d) a pyrite particle (red arrow) and a biomineral (orange arrow).

5.2 Gold grains for Lemmenjoki, Finland

5.1.1 JÄKÄLÄPÄÄ CLAIM

Grains from Jäkäläpää Claim ranged in size from approximately 0.70 to 1.56 mm in diameter. A variety of morphologies were observed including flattened, elongate, equant, irregular and branching Au (Fig. 7a). The grains had sub-rounded to rounded edges, with one almost spherical grain. There were partially folded edges and surfaces can be smooth or uneven. Some grains appeared battered.

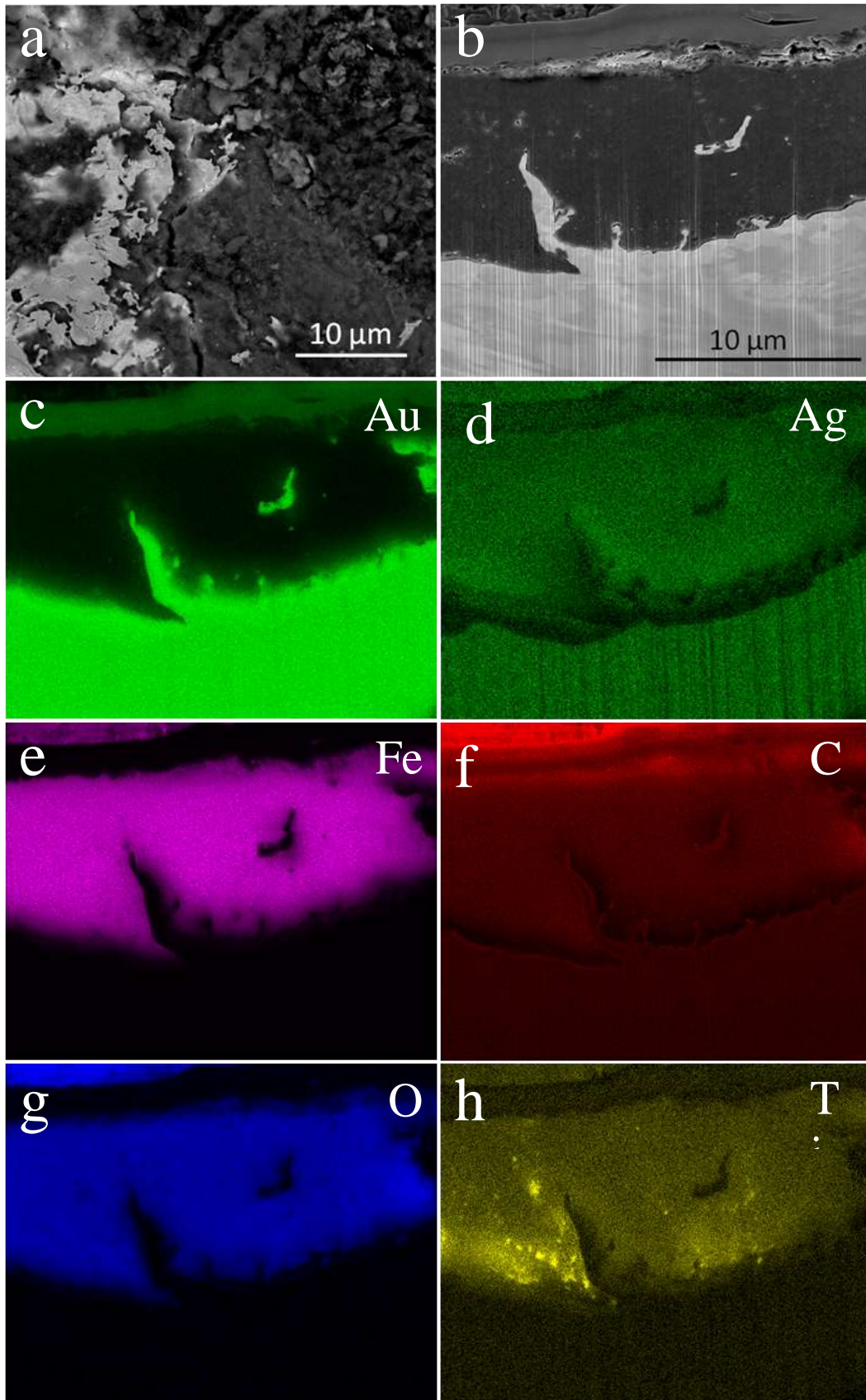


Figure 8: Electron micrographs (a, b) and EDSX maps (c–h) of an Au grain from Jäkäläpää Claim, Lemmenjoki, Finland, showing (a) typical surface features of the grains; (b) FIB-SEM micrograph showing a milled section through a layer of material similar to that shown in (a); (c–d) EDSX maps of Au, Ag, Fe, C, O and Ti concentrations (wt. %) of the milled sections shown in (b).

The grains can be almost completely or partially covered by a polymorphic layer.

Within the layer there was wire-like organic material, Au nano-particles (Fig. 7b) and μ -crystals, which were generally concentrated in regions of high Ti (Fig. 7c). This site had the most extensive Au nano-particles. Single euhedral pyrite particles, approximately 1.5 μm wide, were observed (Fig. 7d). The pyrite were undamaged, showing well defined edges and corners and relatively smooth faces. Biological material, including what appeared to be fungal hyphae, were seen in the polymorphic layer and in direct contact with the grain surface. Biominerals were also observed (Fig. 7d).

An EDXS element map across a milled section of a grain showed Au dispersed through the polymorphic layer (Fig. 8). The Au appeared to be enriched at the grain surface and polymorphic layer interface (Fig. 8c). Silver concentrations also appeared to be depleted in this zone (Fig. 8d). This layer was composed of Fe, O, C, Ti (Fig. 8c–h), Si, Al, Na, Mg and P and can sometimes appear quite thick.

Six Au grains were quantitatively mapped using the Cameca SXFive Electron Microprobe. The element maps across grain interiors showed a variety of Au and Ag concentrations. Grains can show early development of Au enriched rims, whilst others had homogenous Au concentrations across the entire grain (Fig. 9a). Maximum Ag concentrations ranged from 2.52 to 46.07 % Ag. The maximum Ag concentrations occurred in Ag enriched bands through the core (Fig. 9b). These bands had sharp boundaries. Trace elements were also analysed. Minor amounts of S can be throughout grain interiors, as high as 1.40 % S. Along the grain margins Zn, Ti and Fe was observed (Fig. 9c). Elements below detection limit include As. Grains can contain numerous inclusions that ranged in size from 50 to 230 μm .

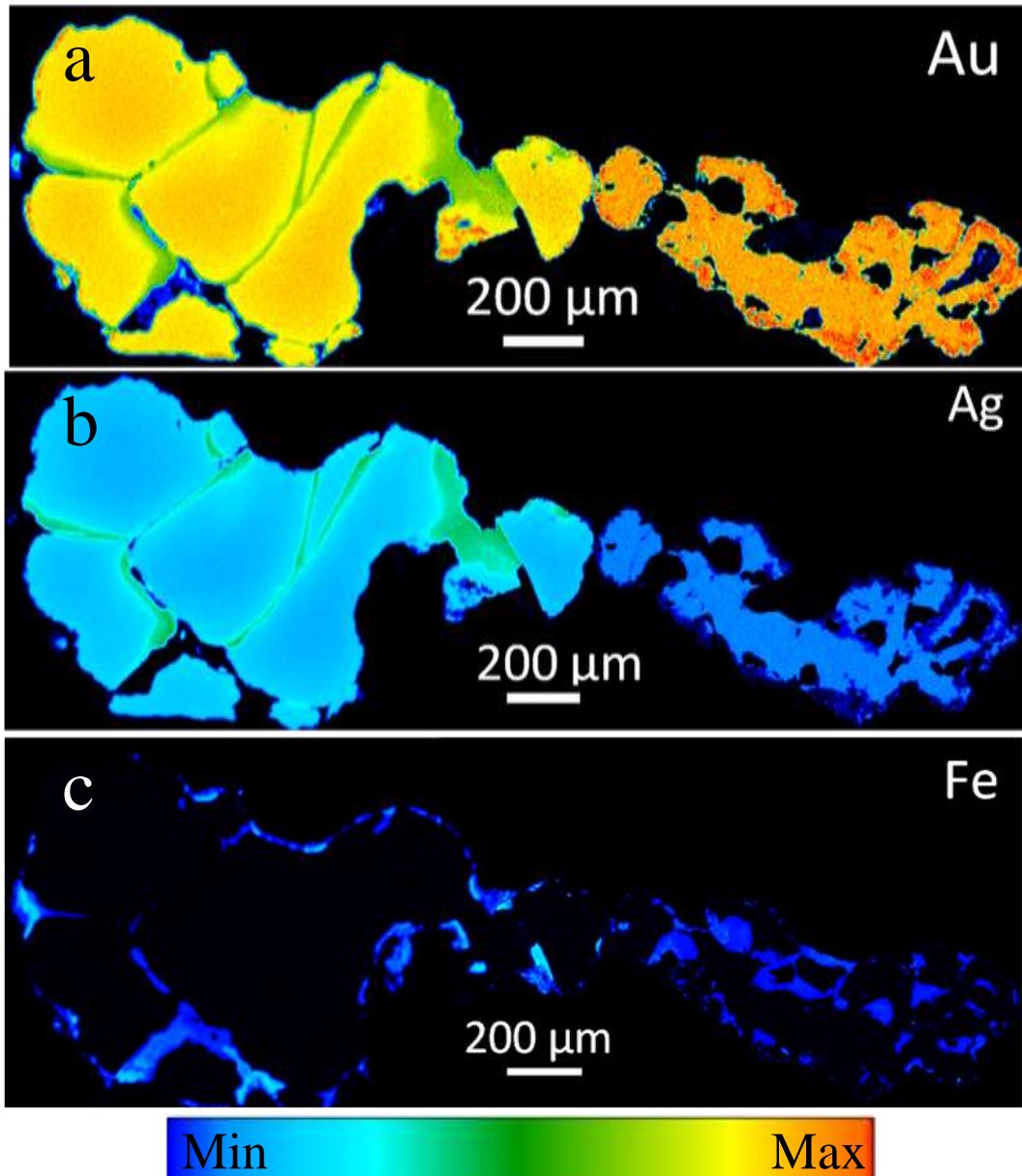


Figure 9: Electron microprobe maps of Au, Ag and Fe concentrations in a polished section of two Au grains from Jäkäläpää Claim, Lemmenjoki, Finland. (a) Maximum concentrations of Au 100 wt.%; (b) maximum concentration of Ag 46.07 wt.%; (c) maximum concentrations of Fe 32.07 wt. %.

5.2.2 (MIESSI) TURKKA'S CLAIM

Grains from (Miessi) Turkka's Claim ranged in size from approximately 0.60 to 1.42 mm in diameter. Grains were elongate, equant or wire grains (Fig. 10a). They had sub-rounded to rounded edges. Linear and curved, randomly orientated scratches were common. Grains can appear to be battered (Fig. 10b).

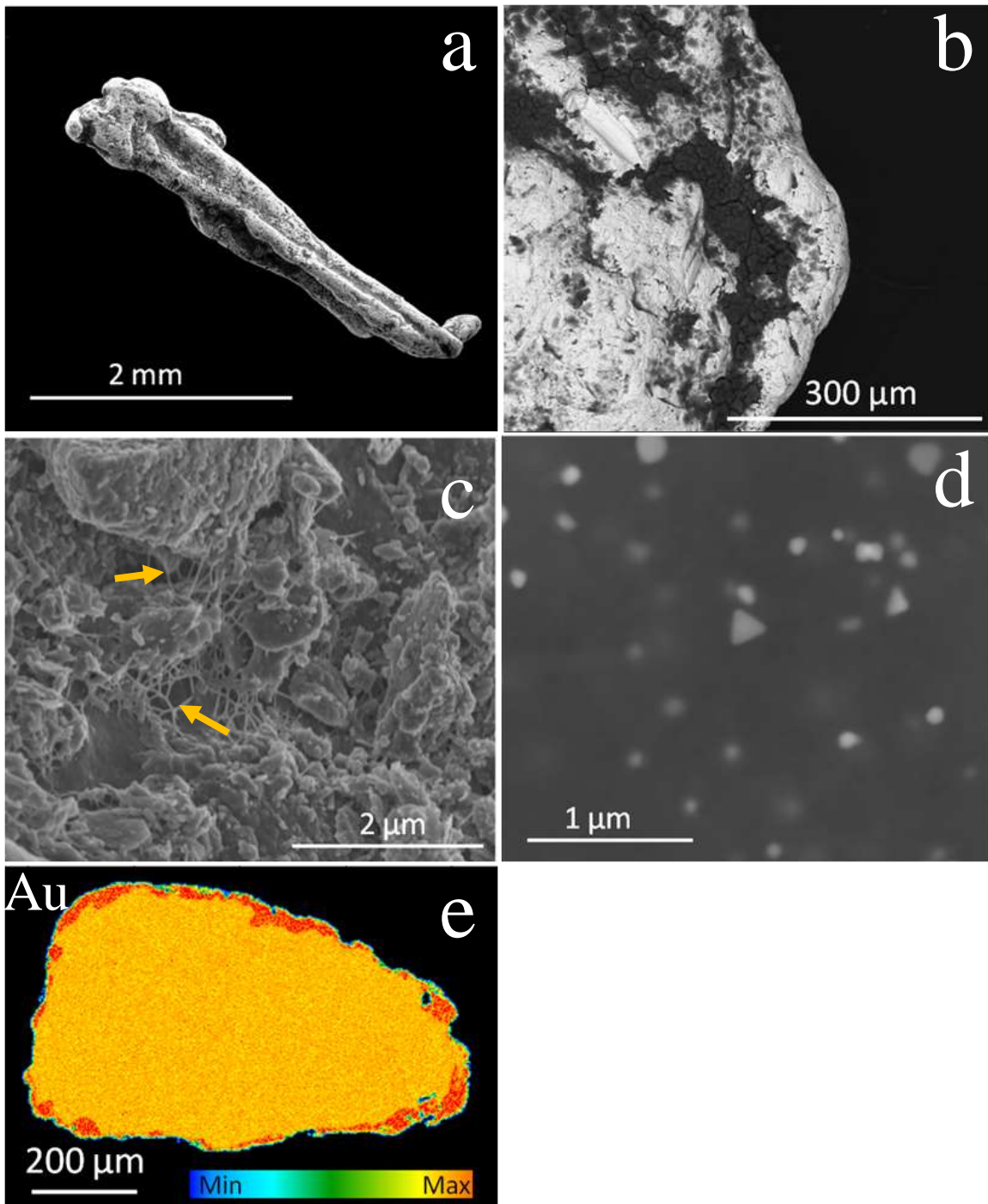


Figure 10: BSE (a, b, d) and SE (c) micrographs and an electron microprobe map of Au grains from (Miessi) Turkka's Claim, Lemmenjoki, Finland showing (a) a wire Au grain with rounded edges; (b) the typical textured grain surface; (c) a network of biological nano-wires (arrows) running through the polymorphic layer; (d) triangular and spherical shaped Au nano-particles; (e) minimum concentrations of Au 60 wt.%, maximum concentrations of Au 100 wt.%.

Grains were almost completely covered or partially covered with a polymorphic layer

(Fig. 10b). This layer was composed of Al, Si, Fe, O, C, Na, Mg, P, K and Ti. Grains

that were almost completely covered by this layer had extensive biological material. Biological nano-wires (Fig. 10c) and singular rod-shaped cells were also observed. The cells can be throughout the polymorphic layer or in direct contact with the grain surface. They ranged in size from 2.5 to 3.5 μm . Putative fungal hyphae were observed in protected, low topography areas.

Nano-particles were dispersed throughout the polymorphic layer, shaped triangular and spherical (Fig. 10d). There was branching Au but it was not as extensive as observed on samples from other sites.

Three element maps across grain interiors showed variation amongst grains. Grains can have irregular enriched Au rims, having concentrations as high as 100% Au and thicknesses ranging from non-existent to 50 μm (Fig. 10e). Grain can have homogeneous concentrations of Au across the entire grain, averaging >98% Au. The Ag content was homogenous in all grains, with concentrations as high as 15.87% Ag. The enriched Au rims can have little to no Ag. Trace elements were also analysed. Elements that were below detection limit include Zn and Cu. Small amounts of As was observed and Ti and Fe can be found on edges. Concentration of S can be as high as 22.07% S. There were inclusions on the edges of the grains.

5.2.3 (MIESSI) PEKKA'S CLAIM

Grains from (Miessi) Pekka's Claim ranged in size from approximately 0.08 to 0.35 mm in diameter. Grains were flattened and can be elongate to equant (Fig. 11a). They had sub-rounded to rounded edges, with some folded edges. There were striations randomly orientated and pits that were filled with matrix. Striations can be linear or curved.

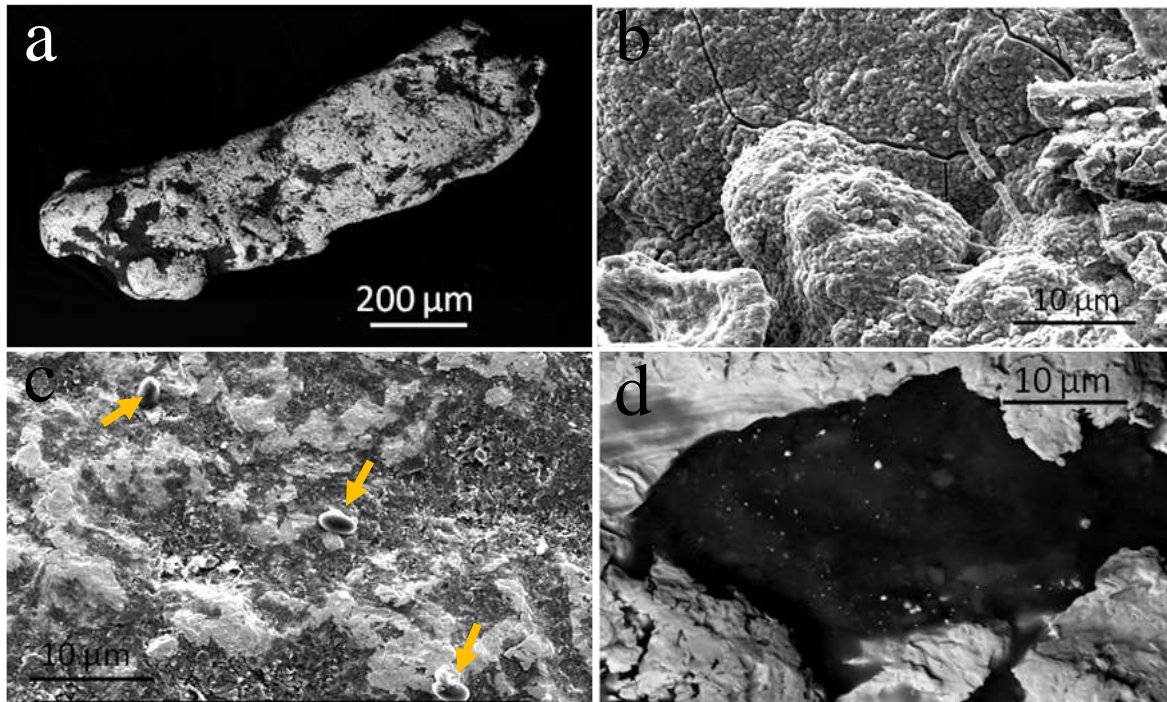


Figure 11: BSE (a, d) and SE (b, c) micrographs of Au grains from (Miessi) Pekka's Claim, Lemmenjoki, Finland, showing (a) an elongate grain with sub-rounded edges; (b) the typical features of the polymorphic layer; (c) bacterial, rod-shaped cells (arrows) on the grain surface; (d) Au nanoparticles dispersed through the polymorphic layer.

Grains were partially covered by a polymorphic layer (Fig. 11b), composed of C, O, Fe, Na, Al, Si and P. This layer can appear quite thick. Singular, rod-shaped bacterial cells were observed on the grain surface (Fig. 11c). Other biological material, Au nanoparticles (Fig. 11d) and μ -crystals were dispersed throughout the polymorphic layer. Branching gold was also observed.

One element map across a grain interior showed lower concentration of Au than grains from other sites. There were partial zones of higher Au at the margins, with a maximum concentration of 95.98% Au. The Au concentration at the core of the grain was >80% Au. Silver was homogenous throughout the core and showed no depletion where Au was highest. The concentration of Ag can be as high as 9.72% Ag in the core. Silver concentrations were lowest at the margins, <5% Ag, creating a consistent rim that mimicked the shape of the grain. Trace elements were also analysed. Traces of Zn and

Cu were along grain margins, reaching maximum concentrations of 0.84% Zn and 0.61% Cu. Thicker zones of Fe also occurred along parts of margins, reaching a maximum thickness of 40 μm and concentration of 39.01% Fe. Elements below detection limit include As and Ti. Inclusions were seen on some grains.

5.2.4 (MIESSI) RAIMO'S CLAIM

Grains from (Miessi) Raimo's Claim ranged in size from approximately 0.60 to 2.00 mm in diameter. Grains can be irregular or branching. They were flattened and have sub-rounded to rounded edges (Fig. 12a). Randomly orientated scratches can be curved or linear (Fig. 12b). Grains can appear battered.

Polymorphic layer material was mostly observed in cavities. Rod shaped bacterial cells were approximately 3 μm in length and can be in clusters or singular (Fig. 12c). Cells can be surrounded by nano-particles (Fig. 12d) and can be in direct contact with the grain surface or in the matrix. Gold nano-particles were dispersed through the polymorphic layer and branching Au can form bridges (Fig. 12e).

Two element maps across grain interiors showed some grains with poorly developed Au enriched rims. The rims can have concentrations as high as 100% Au and have a thickness up to 20 μm . The Au concentration at grain cores can be as low as 86% Au. The grain core can have Ag concentrations as high as 12.41% Ag. Similarly to Jäkäläpää Claim, grains can have bands of high Ag concentrations (maximum 28.93% Ag), that run through the core. The bands had sharp boundaries and had lower Au concentrations. Trace elements were also analysed. Minor amounts of Zn and S were observed on the margins, with much more Fe. Elements that were below detection limits include As and Cu. There can be small inclusions containing Cu, Fe, S.

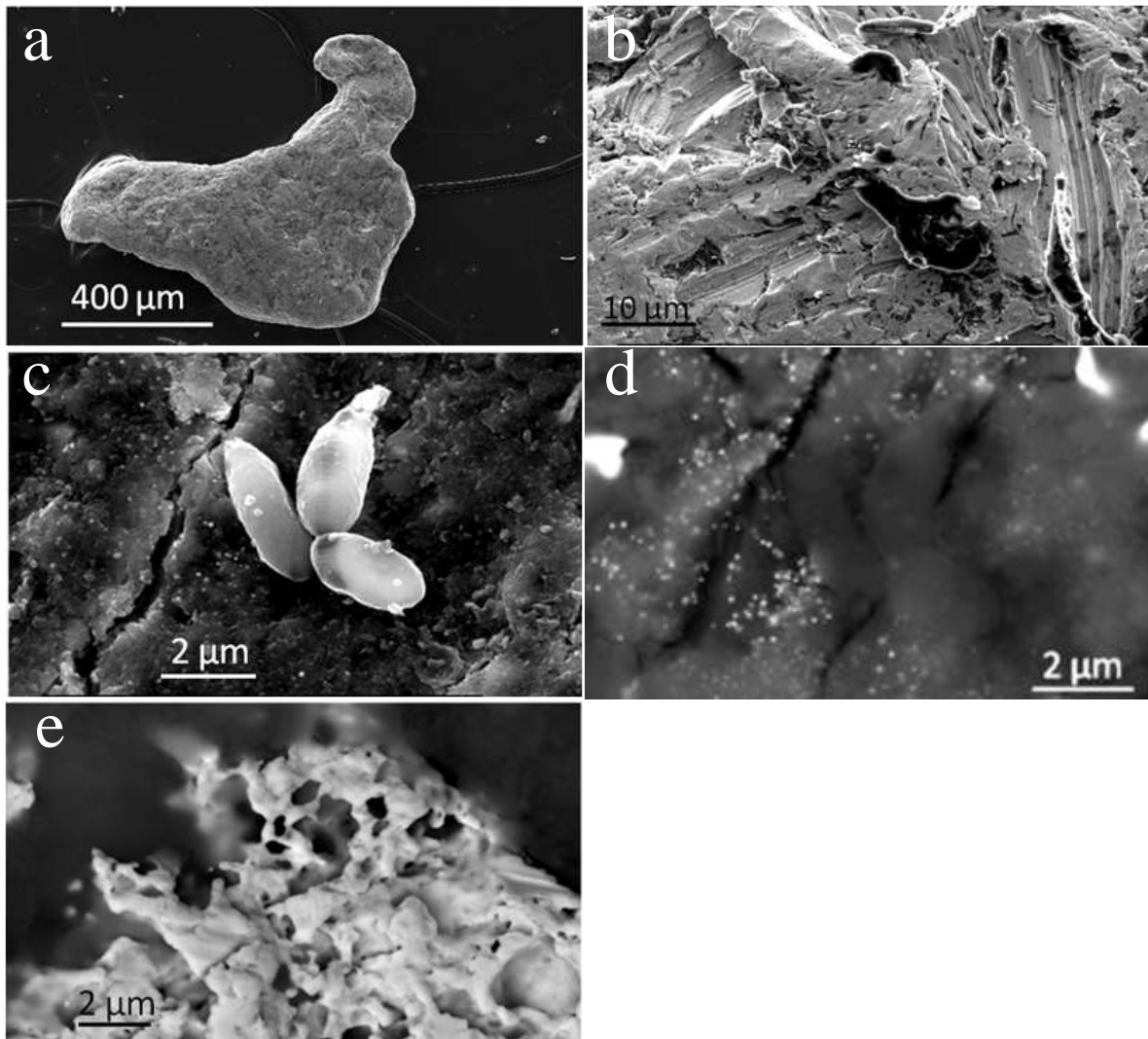


Figure 12: SE (a–c) and BSE (d, e) micrographs of Au grains from (Miessi) Raimo’s Claim, Lemmenjoki, Finland, showing (a) a flattened, branched grain; (b) biological material on the physically damaged surfaces; (c) a cluster of rod-shaped bacterial cells on the surface of the polymorphic layer; (d) the bacterial cells shown in (c) surrounded by Au nano-particles; (e) budding Au forming bridging structures.

5.2.5 KAARREOJA CLAIM

Grains from Kaarreoja Claim ranged in size from approximately 0.45 to 1.20 mm in diameter. Grains can be wire Au and have rounded edges (Fig. 13a). There were curved striations on the grain surface.

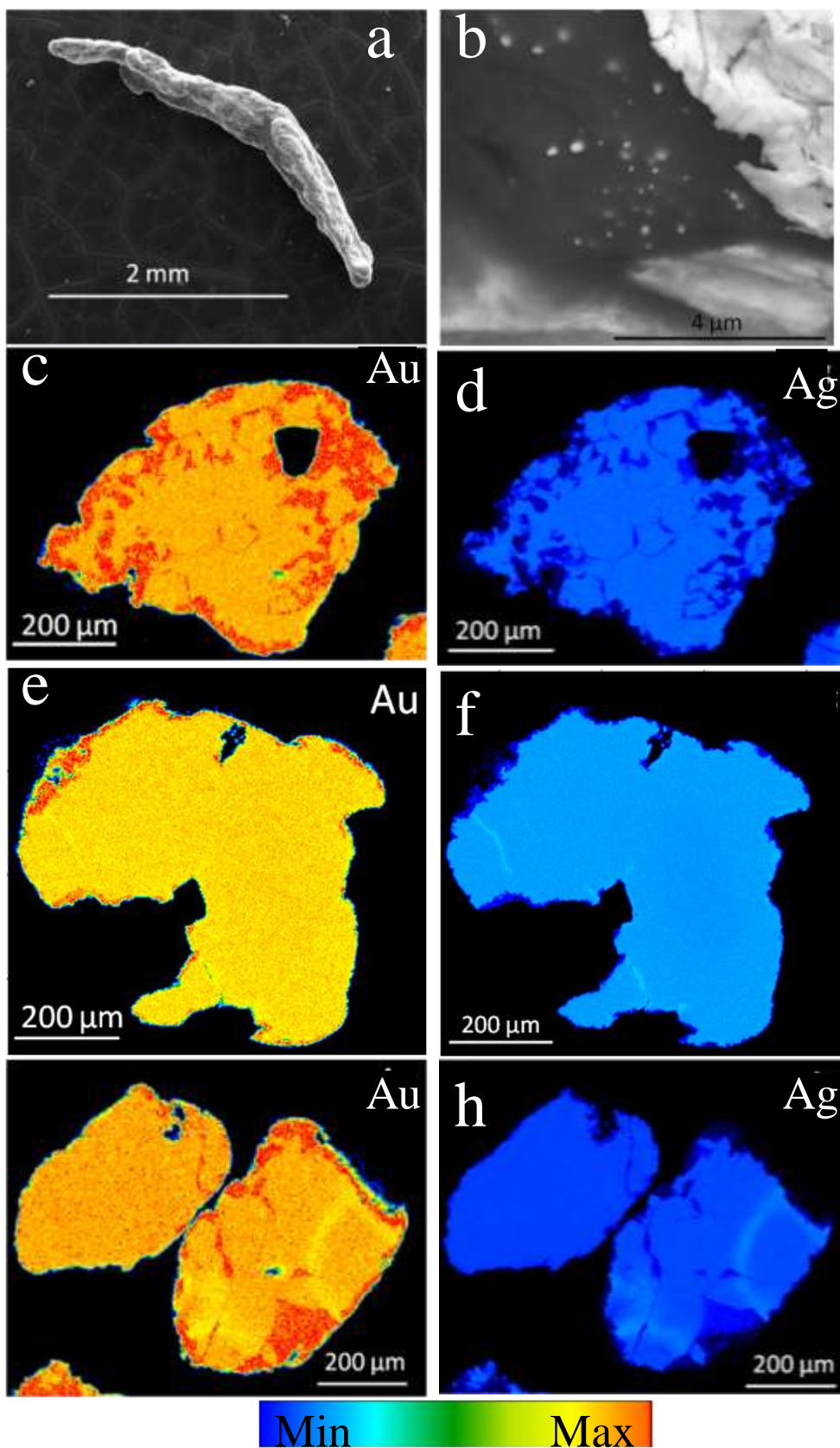


Figure 13: BSE micrographs (a, b) and electron microprobe maps (c–h) of Au grains from Kaarreoja Claim, Lemmenjoki, Finland showing (a) a wire Au grain with rounded edges; (b) Au nano-particles dispersed through the polymorphic layer; electron microprobe maps of Au (c, e, g; maximum concentration 100 wt.%) and Ag (d, f, h; maximum concentration 23.88 wt.%). Note the lack of Ag at enriched Au rims.

A polymorphic layer partially covers grains, again mostly in topographic lows and cavities. The polymorphic layer can contain nano-particles, mostly spherical in shape (Fig. 13b), nano-wires and less common budding Au.

Three element maps across grain interiors showed some grains with poorly developed Au enrich rims and others with irregular patterns (Fig. 13c, e, g). Gold concentrations on the rim of the grains can be as high as 100% Au, with varied core concentrations, always >75% Au. In central areas of the grains, Ag-rich bands up to 40 μm wide were observed, with Ag concentrations up to 18.00% Ag (Fig. 12f, h). The bands boundary can be sharp or diffuse. Core Ag concentrations can be as high as 23.88% Ag (Fig. 13d). Trace elements were also analysed. Minor amounts of S were observed throughout the grains, with concentrations reaching 1.37% S. Grain margins had elevated concentrations of Fe. Elements below detection limit include As, Zn and Cu. Inclusions contained Ti and Fe. Inclusions ranged in size from approximately 10 to 100 μm .

5.2.6 (MIESSI) AMI'S CLAIM

Grains from (Miessi) Ami's Claim ranged in size from approximately 0.80 to 1.55 mm in diameter. Grains had rounded edges but can be irregular (Fig. 14a). There was minor physical damage on surfaces, including few scratches and some battering and folded edges.

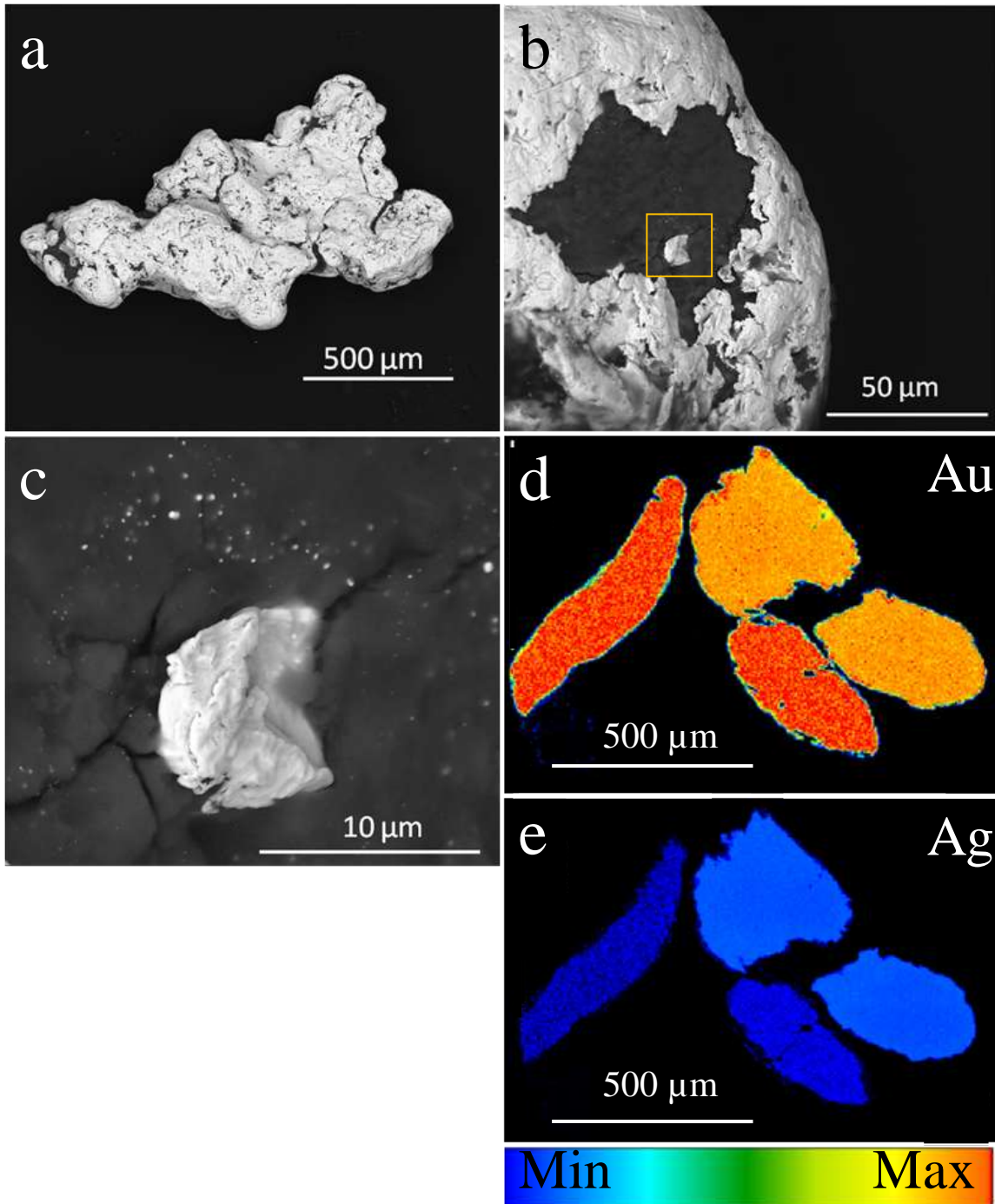


Figure 14: BSE (a–c) micrographs and electron microprobe maps (d, e) of Au grains from (Miessi) Ami’s Claim, Lemmenjoki, Finland showing (a) an irregular Au grain with sub-rounded edges; (b) typical surface features of the grains; (c) increased magnification of Au nano-particles, area highlighted in (b); (d, e) electron microprobe maps of Au (d; maximum concentrations 100 wt.%) and Ag (e; maximum concentrations 11.66 wt.%).

Most of the grains surfaces were exposed, with a polymorphic layer only in the few cavities and topographic lows (Fig. 14b). The layer contained spherical nano-particulate Au (Fig. 14c) and biological material. Budding Au was common and can be bridging

over the matrix. Biological material was also observed on exposed grain surfaces, along with some singular rod-shaped cells.

Four element maps across grain interiors showed homogenous Au concentrations throughout cores, but varying purity amongst grains (Fig. 14d, e). Most of the grains had core Au concentrations >85% Au, but can reach an average >99% Au. Grains can show minor amounts of enriched Au at the margins (Fig. 14d). The Ag content was homogenous across grain interiors but can appear to increase in concentration towards the margins. The Ag content can be as high as 22.12% Ag or as low as <0.5% Ag. The highest Ag concentrations occurred as slightly curved, thin, sharply defined bands that were 10 µm wide, similar to that observed on grains from Jäkäläpää Claim. The bands can run through the entire grain, from margin to margin. Trace elements were also analysed. Concentrations of S can occur at the margins, with maximum values of 2.98% S. Concentrations of Fe also occurred on the margins. Elements below detection limit include As, Zn, and Cu. Internal and exposed inclusions, containing Ti, were observed in grains.

7. DISCUSSION

All Finland grains studied showed signs of physical damage indicative of glacial and alluvial transportation, including rounded and folded edges, striations and cavities. With increased transport, grains become rounded and then flattened and develop smooth, clean to pitted surfaces (Groen *et al.* 1990, Knight *et al.* 1999). Grains studied from sites furthest north from either Ivalojoiki or Lemmenjoiki were irregular and show partially folded edges. Grains from Ivalojoiki become more rounded and eventually flattened as sites changed from glacial till to alluvial. Grains from Lemmenjoiki transgressed from

irregular to elongated and wire Au morphologies from glacial till to alluvial sites.

Randomly orientated striations, observed on most Finland grains, are evidence of physical transport via glacier (Kinnunen 1996).

Pits on grain surfaces can be the result of physical damage (Kinnunen 1996), removal of crystals (Larizzatti *et al.* 2008) or dissolution (Lawrance & Griffin 1994). Many of the pits found on the Finland grains appeared within areas of extensive scratching and are therefore likely to have been obtained through physical damage. However, some of the pits observed on grains from Aila's Claim, in particular, are the result of dissolution (Fig. 5c). Dissolution pits generally produce irregular, mottled surfaces, like the surfaces observed on these grains (Lawrance & Griffin 1994, Falconer & Craw 2009). These surfaces appeared in close proximity to re-precipitation features.

The mobility of metals in the supergene environment may be enhanced by colloids (Weber *et al.* 2009). This is because colloids have a high dislocation content (Hough *et al.* 2008). Gold nano-particles were observed on all grains studied. There have been contrasting views on the formation of nano-particles. It has been linked to inorganic processes, particularly evaporation (Hough *et al.* 2011). However, nano-particulate Au has been observed on grains collected from wet environments, where evaporation is an unlikely influence. Reith *et al.* (2012) suggested that in these conditions, active biogenic processes may facilitate the formation of nano-particles. The presence of Au nano-particles in polymorphic layers (consisting of microbial biofilm and residual biofilm material) observed on grains from Australia (Reith *et al.* 2010, Fairbrother *et al.* 2012) and New Zealand (Reith *et al.* 2012) provides further indication of the importance of biogenic active processes. Similar polymorphic layers observed on Finland grains, and

the arctic climate, suggests that abiogenic processes are the most likely to contribute to the formation of Au nano-particles.

Gold interactions with humic substances have been described as a possible method of colloidal Au formation. Humic acids are capable of reducing Au to its colloidal form, particularly in the hydrosphere (Baker 1978). Of the humic acids, fulvic acids are the most water soluble (dos Santos Jr *et al.* 2005). Fulvic acids are also capable of dissolving Au. They do so by providing potential ligands for Au complexing. (Bowell *et al.* 1993). It is suggested that the acid in solution in the alluvial profile at Risto's Claim is responsible from the dissolution features (Fig. 6c) and minimal Au nano-particles (Fig. 6d) observed on the grains.

Micro-organisms are able to facilitate the solubilization of Au if it can promote Au oxidation and excretes the specific ligands that form complexes with Au (Reith *et al.* 2007). Bacterial cells and/or putative fungal hyphae were observed on most grains studied. An *in vitro* study completed by Reith and McPhail (2006), showed that after 45 days of incubation, microbiota were able to solubilized up to 80 wt. % of native Au. Bacterial cells have also shown to accumulate Au on external cell surfaces and internally (Reith *et al.* 2006). The bacterial cells observed on Finland grains generally appeared in close proximity to Au nano-particles, suggesting a possible influence on particle mobility. The putative fungal hyphae were seen on Au grains from Ivalojoiki 1 and Jäkäläpää Claim and were similar to that observed on grains from New Zealand (Reith *et al.* 2012). Studies have shown that fungi are also able to accumulate Au (Nakajima 2003, Borovička *et al.* 2010).

Gold has a high natural affinity towards itself, promoting the formation of aggregation features (Lawrance 2001). Aggregation features are the result of repeated nucleation of

Au nano-particles, forming chain structures and Au conglomerates, as observed most commonly on grains from Ivalojoiki 1 (Fig 2b; 4b). Continuous re-precipitation of Au via aggregation can result sheets of secondary Au, where the individual particles are still distinguishable (Falconer & Craw 2009). These features are observed on grains from Aila's Claim and (Miessi) Raimo's Claim (Fig. 5e; 12e).

High purity Au-rich rims are indicative of supergene transformation processes. They can form by re-precipitation of Au (discussed above) and/or de-alloying of Ag. Partially developed Au-rich rims were observed on most Finland grains studied. The Au and Ag concentrations appear to be inversely proportional, with little to no Ag where there was Au enrichment.

A number of features favour Au re-precipitation as a method of Au enriched rims.

Supergene Au is generally coarser than grains found from the potential primary material, suggesting growth of grains in the current environment (Reith *et al.* 2007).

There are small inclusions that appear within the enriched Au rim (Fig. 10; 13) and were likely to be incorporated during Au re-precipitation (Groen *et al.* 1990). Supergene Au also displays a number of morphotypes (*e.g.* porous Au, wire and branched Au networks) that are not characteristic of primary Au. The delicate nature of these surface structures could not survive transport (Youngson & Craw 1993).

However, there is evidence to suggest Ag de-alloying is responsible for Au-rich rims.

Grains with irregular core/rim boundaries that create deep embayment into the core, such as a grain from Kaarreoja Claim, Lemmenjoki (Fig. 13c), may be the result of Ag leaching (Youngson & Craw 1993). This feature is explained by a method of Ag leaching is described by Desborough (1970). When Ag becomes oxidised, its size is reduced, resulting in its removal from its site in the alloy. Repetition of this process

creates new Au/Ag alloy interfaces, resulting in porous rims. Some authors suggest that the diffusion of Ag is far too slow to create the sharp boundaries between the enriched Au rim and the core of the grain (Groen *et al.* 1990). However, others argue that the sharp boundary indicates Ag leaching in low temperature conditions (Desborough 1970).

Gold grains from Jäkäläpää Claim, Kaarreoja Claim and (Miessi) Ami's Claim displayed Ag-rich bands through the core. Fairbrother *et al.* (2012) suggest this may be the result of selective leaching of Ag along preferential flow paths or the fusion of multiple smaller grains. Preferential leaching of Ag is preferred because the Ag-rich bands occur mostly in grains with otherwise homogenous cores. (Hough *et al.* 2009). However, some grains have bands that mimic grain boundaries, particularly those from Kaarreoja Claim, Lemmenjoki (Fig. 13h).

Single euhedral pyrite particles were seen on the surface of gold grains from Jäkäläpää Claim. Due to the little physical damage, it is believed that they formed in the surface environment. Pyrite can form through microbial sulfate reduction (Falconer *et al.* 2006). Sulfate reduction can also lead to the formation of Au-thiosulfate complexes (Fitz & Cypionka 1990), which in turn, facilitates the mobilisation of Au. An *in vitro* study completed by (Lengke & Southam 2007), has shown that sulfate-reducing bacteria, in the presence of Au-thiosulfate complexes, were able to precipitate Au from the solution. Sulfate reducing bacteria can be highly active in organic-rich sediments (Winfrey & Ward 1983), and thus, may be an important contributor to the formation of pyrite particles and the complexing of Au in the Finland environments studied.

The core Au and Ag concentrations varied between sites and also between grains from the same site. For example, grains from (Miessi) Ami's Claim can be almost completely

pure Au or can contain more than 10% Ag. Grains that have higher Au overall concentrations generally have experienced greater supergene transformation, where as grains with high Ag content and low rims suggests they have recently been eroded from the primary source (Reith *et al.* 2012). The variance in grains of close proximity may suggest the presence of different Au populations from different primary sources that have now been grouped together as a result of glacial and alluvial transport. The differences between sites may also suggest different primary sources or could reflect differing post-deposition weathering conditions.

Gold grains from Precambrian environments in Australia and Palaeozoic to Oligocene environments in New Zealand have shown to display extensive secondary features (Falconer *et al.* 2006, Fairbrother *et al.* 2012, Reith *et al.* 2012). It has been thought that supergene Au is not common on grains found in locations that were glaciated during the Pleistocene (Wilson 1984). However, northern Finland was glaciated at this time and has been show in this study to not only host supergene Au, but also have grains with secondary features. With increased time, continuous dissolution and precipitation increases the width of the Au-rich rim (Reith *et al.* 2012). Therefore, estimations about the extent of supergene transformation experienced by grains can be made. As expected, grains from the older environments in Australia and New Zealand showed much more developed Au enriched rims than observed on Finland grains. However, as discussed, most Finland grains showed signs of early stages of high purity Au rims, suggesting secondary transformation processes begin not long after deposition.

8. CONCLUSIONS

Deglaciation of Northern Finland began 11,600 years ago, suggesting that supergene Au transformation processes begin not long after deposition. Gold grains studied from

northern Finland's arctic conditions display a range of re-precipitation and dissolution features. The variety of chemical compositions and Au morphotypes on grains from the same site suggests different primary sources. Extensive nano-particulate Au, dispersed through polymorphic layers, and branching Au networks highlight the environmental mobilisation of Au and the subsequent aggregation and re-precipitation onto pre-existing Au particles. Dissolution features and a lack of nano-particles on grains from high organic matter environments suggest that fulvic and humic acids are important contributors in the transformation of Au. Bacterial cells and putative fungal hyphae were closely associated with Au nano-particles. These results show that the model of processes responsible for supergene Au transformation introduced by Fairbrother *et al.* (2012) is also valid in arctic environments. Further research could include trace element analysis to determine possible primary sources or characterisation of the biofilm communities involved in gold cycling in the arctic zone.

9. ACKNOWLEDGMENTS

This study acknowledges the following individuals and institutions for their contributions: The University of Adelaide, CSIRO Land and Water, F. Reith, A. Pring, R. King, K. Howard, J. Zhao and R. Kittle. Equipment and instrument support provided by the South Australian Museum and Adelaide Microscopy. Funding provided by ARC-LP100200102 to F.Reith. Special thanks to Kai 'Mullis' Rantanen, Vasant Mäkinen, Heikki Kalliomannila, Aila Hekkilä and family, Risto and Maija Risto and Maija Vehviläinen, Pekka Turkka, Raimo Kanamäki, Antti Kohtamäki, Sirka and Kari Merentuoto, Ami Telilä, Pekka Itkonen and Pekka Salonen, the Gold Prospectors Association of Finnish Lapland as well as all other friends for their warm welcome, access to sites and the fantastic samples. Thanks also to Manfred and Brigitte Roos, and Tina Khine for help with sampling and sample preparation.

10. REFERENCES

- BAKER W. E. 1978. The role of humic acid in the transport of gold. *Geochimica et Cosmochimica Acta* **42**, 645-649.
- BOROVÍČKA J., DUNN C. E., GRYNDLER M., MIHALJEVIČ M., JELÍNEK E., ROHOVEC J., ROHOŠKOVÁ M. & ŘANDA Z. 2010. Bioaccumulation of gold in macrofungi and

- ectomycorrhizae from the vicinity of the Mokrsko gold deposit, Czech Republic. *Soil Biology and Biochemistry* **42**, 83-91.
- BOWELL R., GIZE A. & FOSTER R. 1993. The role of fulvic acid in the supergene migration of gold in tropical rain forest soils. *Geochimica et Cosmochimica Acta* **57**, 4179-4190.
- CHECA S. K., ESPARIZ M., PÉREZ AUDERO M. E., BOTTA P. E., SPINELLI S. V. & SONCINI F. C. 2007. Bacterial sensing of and resistance to gold salts. *Molecular Microbiology* **63**, 1307-1318.
- DESBOROUGH G. A. 1970. Silver depletion indicated by microanalysis of gold from placer occurrences, western United States. *Economic Geology* **65**, 304-311.
- DOS SANTOS JR D. S., ALVAREZ-PUEBLA R. A., OLIVEIRA JR O. N. & AROCA R. F. 2005. Controlling the size and shape of gold nanoparticles in fulvic acid colloidal solutions and their optical characterization using SERS. *Journal of Materials Chemistry* **15**, 3045-3049.
- FAIRBROTHER L., BRUGGER J., SHAPTER J., LAIRD J. S., SOUTHAM G. & REITH F. 2012. Supergene gold transformation: Biogenic secondary and nano-particulate gold from arid Australia. *Chemical Geology* **320-321**, 17-31.
- FAIRBROTHER L., ETSCHMANN B., BRUGGER J., SHAPTER J., SOUTHAM G. & REITH F. 2013. Biomineralization of gold in biofilms of *Cupriavidus metallidurans*. *Environmental science & technology* **47**, 2628-2635.
- FALCONER D., CRAW D., YOUNGSON J. & FAURE K. 2006. Gold and sulphide minerals in Tertiary quartz pebble conglomerate gold placers, Southland, New Zealand. *Ore Geology Reviews* **28**, 525-545.
- FALCONER D. & CRAW D. 2009. Supergene gold mobility: a textural and geochemical study from gold placers in southern New Zealand. *Supergene environments, processes and products. Econ Geol Spec Publ* **14**, 77-93.
- FINNISH METEOROLOGICAL INSTITUTE 2014. Normal Perids 1981-2010 <<http://en.ilmatieteenlaitos.fi/normal-period-1981-2010>>.
- FITZ R. M. & CYPIONKA H. 1990. Formation of thiosulfate and trithionate during sulfite reduction by washed cells of *Desulfovibrio desulfuricans*. *Archives of Microbiology* **154**, 400-406.
- GROEN J. C., CRAIG J. R. & DONALD RIMSTIDT J. 1990. Gold rich rim formation on electrum grains in placers. *Canadian Mineralogist* **28**, 207-228.
- HOUGH R. M., BUTT C. R. M., REDDY S. M. & VERRALL M. 2007. Gold nuggets: supergene or hypogene? *Australian Journal of Earth Sciences* **54**, 959-964.
- HOUGH R. M., NOBLE R. R. P., HITCHEN G. J., HART R., REDDY S. M., SAUNDERS M., CLODE P., VAUGHAN D., LOWE J., GRAY D. J., ANAND R. R., BUTT C. R. M. & VERRALL M. 2008. Naturally occurring gold nanoparticles and nanoplates. *Geology* **36**, 571-574.
- HOUGH R. M., BUTT C. R. M. & FISCHER-BÜHNER J. 2009. The Crystallography, Metallography and Composition of Gold. *Elements* **5**, 297-302.
- HOUGH R. M., NOBLE R. R. P. & REICH M. 2011. Natural gold nanoparticles. *Ore Geology Reviews* **42**, 55-61.
- KARTHIKEYAN S. & BEVERIDGE T. 2002. *Pseudomonas aeruginosa* biofilms react with and precipitate toxic soluble gold. *Environmental microbiology* **4**, 667-675.
- KINNUNEN K. 1996. Classification scheme for surface textures of gold nuggets from Finnish Lapland. *BULLETIN-GEOLOGICAL SOCIETY OF FINLAND* **68**, 18-33.

- KNIGHT J. B., MORISON S. R. & MORTENSEN J. K. 1999. The relationship between placer gold particle shape, rimming, and distance of fluvial transport as exemplified by gold from the Klondike District, Yukon Territory, Canada. *Economic Geology* **94**, 635-648.
- KOJONEN K. K., TARKIAN M., KNAUF V. V. & TÖRNROOS R. 2005. New results of the placer PGE-minerals from Ivalojoiki and Lemmenjoki rivers, Finnish Lapland. *Extended Abstracts, Geological Survey of Finland*, 145-149.
- LARIZZATTI J. H., OLIVEIRA S. M. B. & BUTT C. R. M. 2008. Morphology and composition of gold in a lateritic profile, Fazenda Pison "Garimpo", Amazon, Brazil. *Journal of South American Earth Sciences* **25**, 359-376.
- LAWRANCE L. M. & GRIFFIN B. J. 1994. Crystal features of supergene gold at Hannan South, Western Australia. *Mineralium Deposita* **29**, 391-398.
- LAWRANCE L. M. 2001. Multi-element dispersion within salt-lake environments: case study of the buried Hannan South gold deposit, Western Australia. *Geochemistry: Exploration, Environment, Analysis* **1**, 323-339.
- LENGKE M. F., FLEET M. E. & SOUTHAM G. 2006. Bioaccumulation of Gold by Filamentous Cyanobacteria Between 25 and 200°C. *Geomicrobiology Journal* **23**, 591-597.
- LENGKE M. F. & SOUTHAM G. 2007. The Deposition of Elemental Gold from Gold(I)-Thiosulfate Complexes Mediated by Sulfate-Reducing Bacterial Conditions. *Economic Geology* **102**, 109-126.
- LUNKKA J. P., JOHANSSON P., SAARNISTO M. & SALLASMAA O. 2004. Glaciation of Finland. *Developments in Quaternary Sciences* **2**, 93-100.
- MCCREADY A. J., PARNELL J. & CASTRO L. 2003. Crystalline Placer Gold from the Rio Neuquén, Argentina: Implications for the Gold Budget in Placer Gold Formation. *Economic Geology* **98**, 623-633.
- MINTER W. E. L., GOEDHART M., KNIGHT J. & FRIMMEL H. E. 1993. Morphology of Witwatersrand gold grains from the Basal Reef; evidence for their detrital origin. *Economic Geology* **88**, 237-248.
- NAKAJIMA A. 2003. Accumulation of gold by microorganisms. *World Journal of Microbiology and Biotechnology* **19**, 369-374.
- NAM S.-H., LEE W.-M., SHIN Y.-J., YOON S.-J., KIM S. W., KWAK J. I. & AN Y.-J. 2014. Derivation of guideline values for gold (III) ion toxicity limits to protect aquatic ecosystems. *Water Research* **48**, 126-136.
- PUUSTINEN K. 1991. Gold deposits of Finland. *Journal of Geochemical Exploration* **39**, 255-272.
- REITH F. & MCPHAIL D. C. 2006. Effect of resident microbiota on the solubilization of gold in soil from the Tomakin Park Gold Mine, New South Wales, Australia. *Geochimica et Cosmochimica Acta* **70**, 1421-1438.
- REITH F., ROGERS S. L., MCPHAIL D. C. & WEBB D. 2006. Biomineralization of Gold: Biofilms on Bacterioform Gold. *Science* **313**, 233-236.
- REITH F., LENGKE M. F., FALCONER D., CRAW D. & SOUTHAM G. 2007. The geomicrobiology of gold. *The ISME Journal* **1**, 567-584.
- REITH F., FAIRBROTHER L., NOLZE G., WILHELMI O., CLODE P. L., GREGG A., PARSONS J. E., WAKELIN S. A., PRING A., HOUGH R., SOUTHAM G. & BRUGGER J. 2010. Nanoparticle factories: Biofilms hold the key to gold dispersion and nugget formation. *Geology* **38**, 843-846.

- REITH F., STEWART L. & WAKELIN S. A. 2012. Supergene gold transformation: Secondary and nano-particulate gold from southern New Zealand. *Chemical Geology* **320-321**, 32-45.
- REITH F., BRUGGER J., ZAMMIT C., NIES D. & SOUTHAM G. 2013. Geobiological Cycling of Gold: From Fundamental Process Understanding to Exploration Solutions. *Minerals* **3**, 367-394.
- SAARNISTO M., TAMMINEN E. & VAASJOKI M. 1991. Gold in bedrock and glacial deposits in the Ivalojoiki area, Finnish Lapland. *Journal of Geochemical Exploration* **39**, 303-322.
- SCHOFIELD E. J., INGHAM B., TURNBULL A., TONEY M. F. & RYAN M. P. 2008. Strain development in nanoporous metallic foils formed by dealloying. *Applied Physics Letters* **92**, 043118.
- SOUTHAM G., LENGKE M. F., FAIRBROTHER L. & REITH F. 2009. The Biogeochemistry of Gold. *Elements* **5**, 303-307.
- STIGZELIUS H. 1977. Recognition of mineralized areas by a regional geochemical survey of the till-blanket in Northern Finland. *Journal of Geochemical Exploration* **8**, 473-481.
- TUISKU P., MIKKOLA P. & HUUMA H. 2006. Evolution of migmatitic granulite complexes: implications from Lapland Granulite Belt, Part I: metamorphic geology. *BULLETIN-GEOLOGICAL SOCIETY OF FINLAND* **78**, 71.
- WEBER F.-A., VOEGELIN A., KAEGI R. & KRETZSCHMAR R. 2009. Contaminant mobilization by metallic copper and metal sulphide colloids in flooded soil. *Nature Geoscience* **2**, 267-271.
- WILSON A. F. 1984. Origin of quartz-free gold nuggets and supergene gold found in laterites and soils — a review and some new observations. *Australian Journal of Earth Sciences* **31**, 303-316.
- WINFREY M. R. & WARD D. M. 1983. Substrates for sulfate reduction and methane production in intertidal sediments. *Applied and Environmental Microbiology* **45**, 193-199.
- YOUNGSON J. H. & CRAW D. 1993. Gold nugget growth during tectonically induced sedimentary recycling, Otago, New Zealand. *Sedimentary Geology* **84**, 71-88.

APPENDIX A: METHODS

Sampling procedure for field sterile sampling of gold grains and regolith to be used for molecular microbial analysis

Modified after Reith *et al.* 2010

Aim of field sterile sampling:

Samples have to be taken field sterile to prevent contamination during sampling and transport. Samples have to be stored on dry ice/ice and frozen to prevent DNA/RNA-degeneration.

Equipment required for field sterile sampling (gold grains and regolith materials):

- Powder free nitrile gloves (do not use latex gloves!)
- Dry ice (ideally) or ice/ice packs if dry ice is not available
- Esky or car fridge
- >70% Ethanol
- Distilled water
- Camping gas burner and gas
- Metal garden shovels
- Role of paper towels

For gold grain sampling:

Gold grains of interest: 0.2 to 2 mm in diameter, preferably secondary gold grains, obtain 25 grains from each sampling site.

Best practise:

If through previous experience it can be assumed that a given regolith material, *e.g.* a concentrate from a sluice, contains a number of gold grains per kg then: pack up the material like any other regolith material (see below), put on ice/dry ice and send to directly to our lab.

If you have to go panning or take samples from a sluice or other form of enrichment device

Additional equipment:

- Gold panning equipment (metal or plastic pan)
 - centrifuge tubes (2 or 10 ml sterile)
 - 1 ml syringes (sterile one-way)
 - Eye wash solution (0.9% NaCl) (important to store gold grains in!!!!)
 - Fine pincers
 - Ideally sterile, distilled water for panning
1. Use gold pan to pan out gold (wear gloves!) use distilled, sterile water if available other water including dam/bore water if necessary.
 2. When gold is visible in the pan use pincers to transfer to centrifuge tube, use one centrifuge tube for each grains

3. Open a new eye wash solution squirt 1-2 ml into centrifuge tube, close tube shake well for 10 sec, open, suck up solution using syringe and discard solution, add new solution so that gold grain is slightly covered.
4. Gold grain is now ready to be put on ice / frozen and send to our lab.

Regolith material sampling for small quantities (50-100g) of sample:

Additional equipment:

- Sterile 50 ml centrifuge (Falcon) tube

Procedure:

1. Obtain samples by opening sterile Falcon tubes immediately before sampling, use Falcon tube to scoop up field fresh regolith sample and close immediately after sampling. Do not touch soil with your hands or other equipment.
2. Collect 2 Falcon tubes full of sample for each site.
3. Put samples on dry ice (if possible, if not use ice) immediately after sampling and transport on dry ice/ice to the lab (see general rules).
4. Send on dry ice/ice to laboratories in Adelaide.

Sample preparation for SEM (dehydration)

Materials:

- EM fixative (4% Paraformaldehyde / 1.25% Glutaraldehyde in PBS, + 4% sucrose, pH 7.2)
- washing buffer (PBS+4% sucrose)
- Ethanol (70%, 90% and 100%)
- Hexamethyldisilazane (HMDS)
- Stubs
- Carbon coating

Procedure:

1. Fix sample for (at least) 30 mins in EM fixative
2. Remove EM fixative and place in a waste bin
3. Wash sample in washing buffer – 1 change, 5mins
4. Dehydrate with
 - 70% ethanol – 1 change, 10mins each
 - 90% ethanol – 1 change, 10 mins each
 - 100% ethanol – 3 changes, 10 mins each
 - HMDS 1:1 with ethanol – 10 mins
 - 100% HMDS – 10mins
5. Remove HMDS and allow to dry
6. Place on stubs
7. Coat the with a 15 nm layer of carbon

Notes: Grains from the same locality were prepared in a single stub. One to six grains were used from each site.

Quanta 450 (FEG Environmental SEM + EDAX TEAM EDS with SDD Detector)

The Quanta 450 was operated in 'high vacuum' mode. The working distance was set at 10 mm. Uncoated, air dried samples and dehydrated, C-coated samples were analysed. Images were collected in secondary electron (5kV, spot 3) and backscatter (20kV, spot 4) imaging mode, with a resolution of 2048 x 1768.

With sites of interest on the grains, several images were taken to characterise the area. Images were also taken at various magnifications (at least 3 different), over the same area, to give a sense of location.

The equipment was equipped with an EDS detector allowing for light element detection. In order to obtain good elemental spectra, the running time was at least 100 seconds.

Philips XL30 FEGSEM x EDAX EDS, Oxford Cyro Stage & HKL EBSD

Set up and basic operations of the Philips XL30 were completed following the Adelaide Microscopy's Phillips XL30 Scanning Electron Microscope Operating Instructions. The working distance was set at 10 mm. Uncoated, air dried samples and dehydrated, C-coated samples were analysed. Images were collected in secondary electron (5kV, spot 3) and backscatter (20kV, spot 4) imaging mode. Images were captured using 'slow scan 3'.

Several images were taken of the site of interest on the grains to characterise the area. Images were also taken at various magnifications (at least 3 different), over the same area, to give a sense of location.

The equipment was equipped with an EDS detector allowing for light element detection. In order to obtain good elemental spectra, the running time was at least 100 seconds.

FEI DualBeam™ Focused Ion Beam (FIB) Scanning Electron Microscope/SEM

Selected samples were analysed using a focus ion beam secondary electron microscope (FIB-SEM; Helios NanoLab DualBeam). Images were collected at 2 to 20kV and 86pA, with sectioning and cleaning at 20kV and 9.7pA.

FEI DualBeam™ has a Gallium ion beam. Before sectioning by the FIB, the area of interest was locally platinum coated to preserve "soft" surface features. Parameters were:

- Pt dep – cold
- Pattern – rectangle
- Value – pt dep
- Application - Si

The instrument was equipped with an Energy Dispersive X-ray Spectroscopy (EDXS); this was used to collect element maps across milled sections. The elements mapped

were: Ag La, Al Ka, Au La, Au Ma, C Ka, Fe Ka, Fe La, Ga Ka, K Ka, Mg Ka, Na Ka, Ni La, N Ka, O Ka, Pt La, Si Ka, Ti Ka.

Mounting and Polishing – preparation for CAMECA SXFive Electron Microprobe w Probe for EPMA Software and Resonetics_LA_ICP_MS

Materials:

- Two-sided tape
- Cover slip
- 2.5 cm plastic blocks
- Epoxy resin
- Vacuum pump
- Razer
- P1200 sandpaper
- 3 μ m and 1 μ m polishing pad
- 3 grade Kemet Diamond Compound
- 1 grade Kemet Diamond Compound
- Ultrasonic cleaner
- Carbon coating

Notes:

Grains from the same locality were prepared in a single mount.

Mounting Procedure:

1. Place two-sided tape on a cover slip, securing a plastic block in the middle
2. Place (number 2-?)gold grains inside, preferably in the middle
3. Completely fill the grey ring with epoxy resin
4. Place in a vacuum pump to remove air bubbles
5. Run several times for a few minutes each
6. Leave to set for a few days
7. Place razer in between tape and peel off
8. Mark grey ring with razor

Polishing Procedure:

1. Start with P1200 sandpaper + water
2. 20 figure 8s, rotate 90°
3. Repeat until at centre of grain
4. Place in an ultrasonic cleaner – 5 mins
5. Use 3 μ m polishing pad + 3 grade Kemet Diamond Compound + water
6. 20 figure 8s, rotate 90°, repeat 10 mins
7. Place in an ultrasonic cleaner – 5 mins
8. Use 1 μ m polishing pad + 1 grade Kemet Diamond Compound + water
9. 20 figure 8s, rotate 90°, repeat 10 mins
10. Place in an ultrasonic cleaner – 5 mins
11. Coat the polished sample with a 15 nm layer of carbon

CAMECA SXFive Electron Microprobe w Probe for EPMA Software

Calibration:

Element/line	Diffracting Crystal	Peak count time (sec)	Background type/fit	Background points (Lo/Hi)	Background count time (Lo/Hi) (sec)	Standard
Au La	LLIF	10	Multipoint	3/2	15/10	Astimex Gold
Cu Ka	LLIF	10	Linear	1/1	5/5	P&H Chalcopyrite
Fe Ka	LLIF	10	Linear	1/1	5/5	P&H Chalcopyrite
As La	TAP	10	Multipoint	1/4	5/20	P&H Gallium Arsenide
Zn Ka	LLIF	10	Multipoint	0/4	0/20	P&H Sphalerite
Ag La	LPET	10	Multipoint	1/3	5/15	P&H Silver Telluride
Ti Ka	LPET	10	Linear	1/1	5/5	Astimex Rutile
S Ka	LPET	10	Multipoint	2/2	10/10	P&H Chalcopyrite

Element/line	Diffracting crystal	Overlapping line/order	Overlap standard
Au La	LLIF	-	-
Cu Ka	LLIF	-	-
Fe Ka	LLIF	-	-
As La	TAP	Fe V, Au VIII	P&H Chalcopyrite, Astimex Gold
Zn Ka	LLIF	Au I	Astimex Gold
Ag La	LPET	Cu III, Hg IV, Au IV	P&H Chalcopyrite, P&H Cinnabar, Astimex Gold
Ti Ka	LPET	Au III	Astimex Gold
S Ka	LPET	Au V, Hg VI	Astimex Gold, P&H Cinnabar

Mapping:

One to three samples were used from each site. Samples were quantitatively mapped using a Cameca SXFive Electron Microprobe running the PeakSite software for instrument control, and Probe for EPMA™ for data acquisition and processing. The SXFive is equipped with 5 WDS X-Ray detectors. Samples were quantitatively mapped using the same peak position, interference corrections, background positions, and calibrated standard intensities as that of spot analysis (Table 1 & 2). The beam condition used for mapping was 20kV and 150nA. Crystals are set to the peak position

of the elements of interest, and the focussed beam was rastered over a set area divided into a specified pixel size:

Dimensions and pixel size

Grains below 50 000 μm^2 = 1 x 1 pixel size

If only 2 grains in sample = 2 x 2 pixel size

Grains $<\sim$ 53 000 μm^2 = 3 x 3 pixel size

Grains $>\sim$ 53 000 μm^2 = 4 x 4 pixel size

Samples were mapped for five elements in single pass maps, and at least one grain from each sample were mapped for eight elements requiring two mapping passes (Table 3). The grains were analysed for (detection limit range in parenthesis in wt.%): Au(0.99-4.83), Ag(0.45-0.49), Cu(0.25-0.61), As(0.43-0.60), Zn(0.33-0.85), Ti(0.09-0.15), Fe(0.18-0.39), S(0.16-0.17). The range in detection limit was due to a variation of counts per second (CPS) across grains.

The time taken for one map is governed by the pixel dwell time (measured in milliseconds), multiplied by the amount of pixels in the given area. For this study the mapped areas ranged in size from 1 by 1 pixels to 4 by 4 pixels, with a dwell time of 50 ms, giving mapping times of approximately 1 to 2 hours. Historically, quantitative mapping is carried out by rastering the beam over the set area with the diffracting crystals on the elemental peak positions, then remapping the same area after offsetting the crystals to a “background” position. This method doubles your acquisition time. The Probe for EPMA software allows fully quantitative pixel by pixel calculation by using the Mean Atomic Number (MAN) background correction (Donovan and Tingle, 1996). This negates the need for remapping the same area to acquire the background intensity.

Quantification and formatting

The MAN background correction and elemental pixel quantification are performed in CalcImage, a module of Probe for EPMA, and false colourisation and formatting done in Surfer™.

Quantitative parameters

Calculate ‘totals’ image

Output detection limits

Net intensities

References

- Adelaide Microscopy’s Phillips XL30 Scanning Electron Microscope Operating Instructions, Adelaide Microscopy, The University of Adelaide
Adelaide Microscopy’s LA_ICP_MS User Instructions, Adelaide Microscopy, The University of Adelaide
DONOVAN, J.J., TINGLE, T.N., 1996. An Improved Mean Atomic Number Background Correction for Quantitative Microanalysis. *Microscopy and Microanalysis*, 1, pp. 1-7.
REITH F., FAIRBROTHER L., NOLZE G., WILHELMIO., CLODE P. L., GREGG A., PARSONS J. E., WAKELIN S. A., PRING A., HOUGH R., SOUTHAM G. & BRUGGER J. 2010. Nanoparticle factories: Biofilms hold the key to gold dispersion and nugget formation. *Geology* 38, 843-846.

APPENDIX B: SUPPLEMENTARY FIGURES



Figure 1: Site photos from Ivalojoiki, Finland (a) Ivalojoiki 1; (b) Aila's Claim; (c) Risto's Claim.



Figure 1: Site photos from Lemmenjoki, Finland (a) Jäkäläpää Claim; (b) (Miessi) Turkka's Claim; (c) (Miessi) Pekka's Claim; (d) (Miessi) Raimo's Claim; (e) Kaarreoja Claim.